NACA RM E54F08

NACA

RESEARCH MEMORANDUM

CHARACTERISTICS OF FLOW ABOUT AXIALLY SYMMETRIC

ISENTROPIC SPIKES FOR NOSE INLETS AT

MACH NUMBER 3.85

By James F. Connors and Richard R. Woollett

Lewis Flight Propulsion Laboratory
Cleveland, Ohio

CLASSIFICATION CHANGED

UNCLASSIFIED

To _____

By authority of _Nasa TPA 9_ Date _9-1-59_

_np 12-1-59_

NATIONAL ADVISORY COMMITTEE
FOR AERONAUTICS
WASHINGTON
August 19, 1954

3320

T-NO

NATIONAL ADVISORY COMMITTEE FOR AERONAUTICS

RESEARCH MEMORANDUM

CHARACTERISTICS OF FLOW ABOUT AXIALLY SYMMETRIC ISENTROPIC

SPIKES FOR NOSE INLETS AT MACH NUMBER 3.85

By James F. Connors and Richard R. Woollett

SUMMARY

An experimental study of the compression fields around axially symmetric isentropic spikes with varying degrees of compressive flow turning was made at a Mach number of 3.85 in order to analyze the basic shock structures and thereby establish further design criteria for supersonic-inlet applications. Pitot-probe surveys and static-pressure distributions along the surface were used in conjunction with extensive schlieren photographs and shadowgraphs to interpret the flow. For zero-angle-of-attack conditions, results are presented for spikes both with and without tip roughness.

For inlets utilizing all-external compression, there appeared to be a practical design limitation on the degree of compressive turning that could be efficiently imposed on the flow. This limit was the amount of turning required to produce a static-pressure rise equal to that across a free-stream normal shock. Over a wide range of Mach numbers (2.0 to 6.0), this criterion satisfactorily predicted the shape and the slope of a curve of current experimental maximum inlet-pressure recoveries. At a Mach number of 3.85, the limiting value corresponded to a final Mach number outside of the boundary layer of 1.95 and a theoretical maximum pressure recovery of 0.74. The difference between this and the experimental maximum inlet recovery (0.62) is largely assignable to frictional and subsonic diffuser losses.

Isentropic survey-spike configurations which exceeded this limit of compressive turning resulted in a reorientation of the shock structure whereby either a bow wave moved out forward of the main shock intersection, or a double-intersection pattern was formed with a strong shock followed by a subsonic expansion field occurring between the two.

INTRODUCTION

A rather extensive investigation of annular nose inlets at Mach number 3.85 has been undertaken at the NACA Lewis laboratory. Earlier results on the performance (pressure, mass-flow, and force data) of several axially symmetric inlet configurations have been analyzed and reported in references 1 and 2. Of those studied, the isentropic inlet indicated the best over-all performance at zero angle of attack as a result of attaining the highest total-pressure recovery without prohibitive external drag. This conclusion was based on a comparison of the specific fuel consumptions and propulsive thrusts of hypothetical ram-jet engines utilizing the various inlet geometries. For the isentropic inlet, a maximum recovery as high as 0.625, corresponding to a kinetic energy efficiency of 0.95, was realized. However, this value was still far below a theoretical maximum recovery of 0.92 which was based solely on normal shock losses after assuming inviscid flow and isentropic compression to Mach number 1.5.

In view of the large discrepancy between experiment and theory, the present investigation was undertaken to ascertain the basic underlying factors contributing to such a difference. Specifically, the objectives of this study were (1) to survey and analyze the basic shock structures and the flow fields around the isentropic spike at Mach number 3.85; (2) to establish, at least qualitatively, a breakdown of the losses associated with this particular type of design; and (3) to indicate possible direction in changing the design procedure in order to attain further improvements in over-all performance.

Experimentally, the flow fields of isentropic spikes with various degrees of compressive flow turning were surveyed by means of a traversing pitot probe and wall static-pressure distributions. The results of these pressure data were supported by both schlieren photographs and shadowgraphs of the corresponding shock patterns. In addition, the investigation was conducted both with and without the application of roughness to the spike tips, and only zero angle of attack was considered.

SYMBOLS

The following symbols are used in this report:

M   Mach number

P   total pressure

p   static pressure

K.E.   kinetic energy efficiency defined as ratio of kinetic energy available after diffusion to kinetic energy in free stream,

$$1 - \frac{2}{(\gamma - 1)M_0{}^2}\left[\left(\frac{P_0}{P_3}\right)^{\frac{\gamma - 1}{\gamma}} - 1\right]$$

γ ratio of specific heats for air

λ_{max} maximum two-dimensional flow turning angle for attached flow

Subscripts:

0   free-stream conditions

1   conditions in survey plane at main shock intersection

3   conditions at end of subsonic diffuser

B   conditions behind normal shock

f   final conditions outside of boundary layer

x   local condition

APPARATUS AND PROCEDURE

The experimental program was conducted at a Mach number of 3.85 in the Lewis 2- by 2-foot supersonic wind tunnel. Test-section conditions corresponded to a simulated pressure altitude of approximately 108,000 feet and a Reynolds number per foot of approximately 1.03×10^6. Tunnel air was maintained at a stagnation temperature of $200\pm5^\circ$ F and at a dew-point temperature of $-20\pm10^\circ$ F.

In figure 1(a), a photograph is presented to show a general over-all view of the isentropic inlet (5-in. maximum cowl diameter) installed in the tunnel test chamber. The entire configuration is the same as that of references 1 and 2. In table I pertinent dimensions of the isentropic inlet and survey spikes are listed. For the survey study, the inlet cowl was removed and the exposed blunt lap-joint was concealed behind a sharp-edged ring. A close-up photograph showing the isentropic spike and pitot-probe survey arrangement is given in figure 1(b). Probe tip dimensions are presented in the schematic sketches of figure 1(c). For convenience the isentropic spike of reference 1 will hereinafter be referred to as the original spike, as contrasted with the survey-spike configurations.

As illustrated in the drawing of figure 1(d), the contours of the original and survey spikes were somewhat different in scale; however, the two spikes were otherwise geometrically similar.

The contours of the isentropic spikes were designed by the method of characteristics (ref. 3) to focus all the compression waves at a point located out on the conical tip shock. At this focal point, a two-dimensional compressive flow turning (reverse Prandtl-Meyer streamline) was assumed to occur. The initial cone had an 8° half-angle, and the surface was not corrected for boundary-layer growth. The calculation upon which the experimental contours was based employed a two-dimensional turning of finite radius and did not involve any iterations in the solution. In the subsequent analysis of the survey data, some discrepancy existed between the experimental and theoretical final Mach numbers after compression occurred. To check this discrepancy, a more refined calculation was made wherein several iterations were made in the solution for each point in the characteristics network and a zero-radius point-turning was assumed on the initial tip shock. The results of these two methods are indicated in figures 1(e) and (f). As shown, there was a negligibly small difference involved between the geometric contours but rather appreciable changes in the local Mach number distributions along the spike, particularly at the larger surface angles. Since the later refined calculation was corroborated by the data, this Mach number distribution (fig. 1(f)) will be used in the subsequent discussion. Thus, the original spike instead of having a theoretical final Mach number of 1.5 was theoretically capable of compressing the flow only down to a Mach number of 1.75, and a corresponding total-pressure recovery of 0.826.

Similarly the survey spike was based on the same theoretical contour and was designed to carry the compression initially down to a Mach number of 1.73. With successive maching operations to modify the spike shoulder (fig. 1(g)), several amounts of compressive flow turning were obtained. These various steps corresponded to theoretical final Mach numbers of 1.73, 1.77, 1.89, 2.06, 2.25, and 2.45 and were designated as configurations A through F, respectively. As illustrated in figure 1(f), two survey spikes were fabricated with different types of shoulder modification downstream of the design point. The first employed an immediate constant-radius expansion after the design point (configuration designation unprimed); the second had a small-pressure-gradient conical surface following the design point (configuration designation primed). The second type was used in the pitot-probe survey study.

In order to study further the effects of an artificially induced transition from laminar to turbulent boundary layer upon the main flow fields, the isentropic spikes were also investigated with roughness. This was done by applying a 1/2-inch band of (No. 60) carborundum grit to the spike tip. Configurations with tip roughness are designated by the letter R.

To actuate the pitot probe, a small electric motor and screw arrangement was used. As shown in the photograph of figure 1(b), the probe

3520

traversed a survey line perpendicular to the spike axis of symmetry. An
electric contact indicator was employed to establish the vertical zero
reference position of the probe. Manual adjustment for axial location
was also provided.

Additional pressure instrumentation consisted of approximately 25
static-pressure taps distributed axially along the spike surface. At the
exit of the subsonic diffuser of the isentropic inlet, an extensive pres-
sure rake was used to indicate the inlet total-pressure recovery (see
ref. 1). Optical provisions for observing the shock patterns in the flow
included a twin-mirror spark schlieren system and a spark shadowgraph
system.

For probing along a specific line in the flow field, for example,
one passing through a particular shock intersection, the axial station
was determined through observation with the schlieren or shadowgraph ap-
paratus. The inclination of the probe-tip was determined by the surface
angle of the spike at the survey station. Data were recorded as the probe
traversed between the spike surface and a point well outside the compres-
sion field. For use in the analysis, measurements of the various flow
angles were taken from schlieren and shadowgraph pictures enlarged to
approximately four times full scale.

RESULTS AND DISCUSSION

For clarity and continuity of development, this section of the re-
port has been subdivided under three major headings. The first, "Origi-
nal Isentropic Spike and Cowl," considers the flow characteristics of a
current high-performance isentropic inlet. The second, "Isentropic
Survey-Spike Configurations," presents the results of an extended study
of the compression characteristics of a family of isentropic spikes having
various amounts of turning above and below that of the original inlet con-
figuration. Finally, the third subdivision, "External-Compression Limita-
tions," concerns the conclusions or deductions derived from these studies
and their extrapolation to other Mach numbers. This last section includes
a new viewpoint which indicates that the performance capabilities of
external-compression inlets may be limited to values much lower than
heretofore anticipated.

Original Isentropic Spike and Cowl

Inlet performance. - Static-pressure distributions along the center-
body surfaces of the isentropic inlet during supercritical operation are
presented in figure 2. As the back pressure was increased by progres-
sively restricting the sonic exit area, the diffuser shock moved forward
and the total-pressure recovery increased to a maximum of 0.574. At this
condition the shock was located close to the cowl lip as demonstrated by
the static pressures. The distributions, in general, indicated that the

subsonic diffuser was performing satisfactorily insofar as there was no evidence of local separations of the flow that might limit the forward positioning of the normal shock configuration. However, the static-pressure level at the minimum area (entrance) was somewhat below that expected from the theoretical design (theoretical $p_x/P_0 = 0.18$; experimental $p_x/P_0 \approx 0.16$). Approximately 5 to 6 inches from the spike tip, there was a flat (zero pressure gradient) portion in the distribution curve, indicating laminar boundary-layer separation and subsequent reattachment. A corresponding schlieren photograph of the inlet-flow pattern (shown as an insert on the figure) illustrates further the extent of separation and its effect on shock structure and also the location of the various shocks relative to both the spike and cowl. These shocks will be described in more detail in the subsequent discussion.

Visual flow observations for spike alone. - In order to isolate the supersonic portion of the diffuser for detailed study and to evaluate the performance of the external-compression surface independent of the remaining inlet geometry, the cowl was removed. Resultant flow patterns of the compression fields are presented in figure 3 for the spike with and without tip roughness. For clarity, the nomenclature to be used throughout this paper is given in figure 3(a). Shock S for the no roughness case is the shock which appears to form in the vicinity of the separation point and is strengthened by the coalescence with weaker upstream shocks. As shown here and in all the subsequent photographs, the application of tip roughness apparently eliminated boundary-layer separation. The shock configurations in the vicinity of the main intersection were quite similar for the roughness and no roughness cases.

Photographic enlargements of the main shock intersections are presented in figure 4. The shock formation consisted of a single-intersection branch shock structure, the upper leg being of the strong shock family. In order to satisfy the condition of a pressure balance across the vortex sheet, a shock reflection was necessary.

The angles of the vortex sheets immediately behind the main shock intersections were measured as being equal to or slightly greater (up to approximately 6°) than the maximum deflection angle corresponding to the free-stream Mach number ($\lambda_{max} = 38.2^\circ$). A solution compatible with such angular measurements (in excess of λ_{max}) is that the upper leg of the branch configuration was actually a bow wave. This possibility was checked against the approximation of reference 4 by considering the contour of the vortex sheet analogous to that of a blunt body in a flow at free-stream Mach number. Agreement was only fair, but probably within the accuracies of the method and the angular measurements. However, there also existed the possibility that, since the main shock intersection itself was not precisely defined in the photographs, all the shock waves may not have fallen exactly on a single focal point of intersection. Thus, knowledge of the flow structure may have been obscured and limited by the resolving power of the optical system.

3320

To illustrate the extent of the influence of probe disturbances on the flow fields, typical photographs of the largest pitot probe in survey positions are shown in figure 5. The effect appeared small. Subsequent surveys were made with probe tips of one half this size.

Pressure and Mach number profiles. - Profiles of the flow along a survey line through the main shock intersection and perpendicular to the spike axis are presented in figure 6. The pitot-pressure profile (fig. 6(a)) indicated a maximum pressure recovery $(P_{x,B}/P_0)$ of 0.73 with a mean value obtained through an area integration from the wall out to the main shock intersection of 0.64. This value of 0.64 roughly checked with the maximum over-all inlet recovery of 0.574 by allowing the difference to be attributed to subsonic diffuser losses.

Mach number and total-pressure profiles (fig. 6(b)) were calculated by applying the Rayleigh and other normal-shock equations to the measured pitot pressures and a static pressure, which was assumed to hold constant from the spike surface out to the main shock intersection. This assumption was deemed to be reasonably valid after an inspection of the theoretical characteristics diagram revealed very small changes in Mach number from the surface to the intersection - in this case, approximately 1.75 to 1.74. Outside of the boundary layer, the final Mach number was approximately 2.0 with nearly isentropic compression being indicated by total-pressure ratios close to unity. This Mach number was well above the design value of 1.75. However, these conditions plus an approximate 2° compression (as a shock reflection) roughly satisfied the strong shock pressure rise across the upper leg of the branch shock configuration, thus providing the required pressure balance across the vortex sheet.

In order to investigate further the extent of the boundary-layer separation off the spike and its effect on the main flow field, a pitot-pressure survey was made through the separation zone at a station 5.8 inches from the spike tip. Without tip roughness (fig. 7(a)), the thickness of the separated region was clearly defined and was approximately 0.035 inch as indicated by the cross-hatched band. With the application of tip roughness (fig. 7(b)), this separation was eliminated. It was also observed that the mean values of the pressure ratio $P_{x,B}/P_0$ at this station were approximately the same for both the roughness and no roughness cases even though the distributions across the flow field were quite different.

In analyzing the branch-shock configurations of the original isentropic spike, it was evident, from the viewpoint of inlet application, that further systematic research should be directed toward studying various amounts of external compressive turning for the purpose of optimizing the performance of this type of inlet. With this aim, the isentropic spike survey program was undertaken.

Isentropic Survey-Spike Configurations

Visual flow observations. - Based solely on isentropic compressive
flow turning with characteristics focussed at a point on the initial tip
shock, the theoretical design variables of final Mach number and surface
angle are tabulated on figure 1(e). Varying degrees of compression above
and below that of the original spike were incorporated in the design. The
resulting flow patterns obtained for the various configurations with and
without roughness are shown in the schlieren photographs and shadowgraphs
of figure 8. For configurations A, B', and C' without roughness (figs.
8(a), (b), and (c), respectively), double-intersection solutions were
obtained wherein the upper one was designated as the shock-S intersection
and the lower one as the main shock intersection. As can be observed in
the photographs, the vortex sheet from the shock-S intersection had a
pronounced curvature immediately downstream of the intersection before
it paralleled the lower vortex sheet. The angles of these trailing vortex
lines attained maximum values of approximately 45° with the axis of the
spike ($\lambda_{max} = 38.2^\circ$). With decreasing turning, that is, progressing from
A toward C', the annular distance between the two intersections was ob-
served to decrease.

With the application of roughness to the spike tip, configurations
A(R), B'(R), and C'(R) were found to have definite bow waves formed out
ahead of the main shock intersection. Again, the bow-wave relations
given by the approximation of reference 4 were applied and found to hold
reasonably well. In addition, it was noted that the upstream displace-
ment of the bow wave ahead of the main shock intersection decreased with
decreased turning from A(R) to C'(R).

In figures 8(d), (e), and (f) the flow patterns obtained with con-
figurations D', E', and F', respectively, with and without tip roughness
are shown. In each case, single-intersection weak two-dimensional branch
shock formations resulted. As would be expected, the angles of the vortex
sheets and the shocks downstream of the intersection decreased with de-
creased turning. The application of tip roughness did not appreciably
alter the basic shock structures immediately downstream of the main-shock
intersections.

For the configurations with constant-radius shoulder, expansion
waves emanating from the spike surface immediately after the design point
produced a marked change in the shock pattern when compared with that
obtained with a conical section after the design point. This change is
illustrated quite clearly by comparing the patterns for configuration C
with and without roughness (fig. 8(g)) to those of configuration C' (fig.
8(c)). This effect precluded the accurate interpretation of the survey
data in that the traverse line of the probe would then have to pass
through a nonuniform static-pressure field. Consequently, all pressure-
survey data were taken with configuration modifications of the conical
small-pressure-gradient type.

3320

CW-2

        Pressure and Mach number profiles. - Pitot-pressure profiles in a
survey line perpendicular to the axis and passing through the main-shock
intersections (indicated in fig. 8(a)) are presented for the various
isentropic survey-spike configurations in figure 9. The vertical lines
and arrows on the figures indicate the shock intersections as measured
from corresponding shadowgraphs. Generally, it was found that the appli-
cation of tip roughness resulted in slightly higher pitot pressures.
With the exception of configuration A, the maximum values of $P_{x,B}/P_0$
decreased with decreased turning. The highest value of 0.84 was attained
with configuration B'(R). For the double-intersection solutions (con-
figurations A, B', and C'), low-pressure-recovery air was encountered
between the main and shock S-intersections. In every case, the thick-
ness of the boundary layer at the survey plane was approximately 1/8
inch and represented a large portion of the annulus of air (in some cases
more than one third of the height) between the spike surface and the
main shock intersection. Within this boundary layer, an irregularity in
the profile (approximately 0.05-in. from the surface) became evident with
configuration C' and became more pronounced with decreased compression
from C' to F'. The reason for this irregularity is at present unknown.

        In figure 10, the static-pressure distributions along the surfaces
of the various isentropic survey-spike configurations with and without tip
roughness are presented. Enough data points were plotted to establish
the experimental curves and to indicate the order of scatter. Also in-
cluded is the theoretical distribution based on the characteristics so-
lution. Generally fair agreement between experiment and theory was ob-
tained with regard to the shape of the curve; however, all the experi-
mental data tended to fall somewhat higher than the theory except for
a short range in the no-roughness case immediately following the laminar-
boundary-layer separation region. Slightly higher pressure levels were
realized along the spike for the tip roughness cases, except in the
separation region of the no roughness case. This separation zone was
clearly defined, for the no roughness configurations, by a flat section
in the distribution curve. The angle between this separation boundary
and the axis of symmetry was approximately 19° as determined by measure-
ments from a large number of schlieren photographs. As seen from the
data, pressures upstream of the design points were unaffected by down-
stream shoulder modifications.

        Mach number and total-pressure profiles (fig. 11) were again cal-
culated from the survey pitot pressures and the wall-static pressure
which was assumed to hold constant throughout the compression field.
Outside the boundary layer, the Mach numbers conformed adequately to the
theory for all survey-spike configurations. In general, the data in-
dicated nearly isentropic compression in the center of the high-
compression fields with total-pressure ratios near unity. For

configurations A, B', and C'; subsonic-flow fields were indicated
between the main and shock S-intersections; however, the static-pressure
used in the calculation of Mach number in this region was somewhat
high.

Flow analysis of double-intersection shock structure. - Based on the
pressure-survey data and angular measurements from enlarged schlieren
photographs, a two-dimensional flow analysis was made of a typical double-
intersection shock structure (configuration A). A schematic representa-
tion of the flow is given in figure 12. The static-pressure levels in
the various fields and also the basis for calculation of the different
values are indicated in the inserted table.

The requirement of a pressure balance across the vortex lines led
to the following conclusions: The flow field between the vortex lines
downstream of the main and shock S-intersections was essentially a
subsonic flow behind a strong (normal) shock reaccelerating to choking
at station 5, as labeled on the sketch. This interpretation was sup-
ported by the curvature of the upper vortex line before it became paral-
lel to the lower one and by the area contraction in the channel formed
between the two vortex lines, as seen in the schlieren photograph (fig.
8(a)). To satisfy the pressure requirement at the upper vortex line
just behind the shock S-intersection, the normal shock between zones 2
and 4 could bifurcate somewhat in the manner shown. This effect cannot
be distinguished in the photographs except as a blurred region since it
occurred in a very small area. Theoretically at least, the flow from
zone 3 would pass through the downstream leg of the branch shock and
enter zone 4 to 5 at near sonic velocity. A 5° to 6° compression wave
(as a shock reflection) served to provide the necessary pressure balance
across the lower vortex line. Thus, in this rather complicated shock
structure, the following static-pressure levels were encountered: in
the survey plane outside the boundary layer ($p_7/P_0 \sim 23.5$), downstream
of main shock intersection ($p_4/p_0 = p_6/p_0 \sim 30$), and downstream of the
shock S-intersection ($p_1/p_0 = p_3/p_0 = p_5/p_0 \sim 17.5$). Although this large-
ly qualitative discussion appears to describe this type of shock structure,
no satisfactory description exists for the theoretical inviscid flow case
of high compressive turning with resulting mixed-flow fields.

As observed earlier in the discussion of the shock patterns (fig. 8),
the two intersections tended to approach each other with decreased com-
pressive turning. Thus, in the limit, superposition of the main and shock
S-intersections might be attained. This condition appeared to be nearly
achieved with the original isentropic spike.

Shock-intersection locations. - The relative positions of the shock
intersections encountered in the survey plane for the various configura-
tions are presented in figure 13. Main shock intersections appeared to

3320

CW-2 back

fall along a 45° line with a trend to move back from the tip and out from the axis with decreased compressive turning. This 45° line appeared to be approximately at the angle of the final coalesced shock waves. As shown on figure 13, the design focal point of the compression waves also fell on this line and close to that of configuration A. With decreased turning, the decrease in the annular distance between the main and shock S-intersections for configurations A, B', and C' is again illustrated.

Potential inlet-pressure recoveries. - A summary of the potential pressure recoveries available for all-external-compression inlets designed to accommodate the flow fields of these various isentropic survey spikes is presented in figure 14. All the experimental data points represent values obtained through area-weighted integrations of the survey profiles given in figure 9. The solid-line values are indicative of the performance capabilities of hypothetical inlets having cowls located at the main-shock intersections of configurations D', E', and F' with and without tip roughness. As such, these inlets would have relatively uniform profiles at the entrance and no supercritical flow spillage (capture mass-flow ratio of unity). The single-dashed-line values are for hypothetical inlets having cowls located at the main shock intersections of configurations A, B', and C' with and without tip roughness. Although benefitting from pressure recoveries higher than the solid-line values, these inlets would be penalized by mass-flow spillage and attendant additive drag. For the no-roughness cases, this mass-flow spillage was estimated at 5 to 6 percent of the maximum capture mass flow. With configurations A, B', and C', there was the alternative of avoiding this mass-flow spillage by locating the inlet cowls at the shock S-intersections; the resulting available pressure recoveries are indicated by the double-dashed line values on figure 14. Although there would be no supercritical spillage, these latter inlets would be penalized by non-uniform profiles at the entrance with concomitant mixing losses and, more importantly, with no gain in recovery above the solid-line values.

External-Compression Limitations

Mach number 3.85. - In the analysis of these various shock structures, it was observed that the required condition of balancing the static pressures across the vortex sheets (neglecting flow direction) might impose a limit upon the amount of external compression attainable, this limit being set by the maximum pressure rise through a single shock, that is, the normal shock. This proposed limitation was converted into a limiting final Mach number along the compression surface (see appendix) and superimposed on the data of figure 14. As illustrated, this Mach number limit (M_f = 1.95) subdivided the experimental data quite well in that the configurations with excess compressive turning incurred penalties of mass-flow spillage and additive drag which appeared to offset the gains

in pressure recovery above that at the limiting value. For a free-stream
Mach number of 3.85, this limiting condition for all-external-compression
inlets corresponded to a final Mach number outside the boundary layer of
approximately 1.95 and a theoretical pressure recovery of 0.74. This
concept, derived from experimental observations, may then constitute a
practical design limitation, applicable to all-external-compression inlets
where mass-flow spillage and attendant additive drag are weighed in over-
all performance. An adequate theoretical description of the shock struc-
tures and mixed-flow fields when this limit is exceeded has not yet been
devised.

Variation with Mach number. - This proposed limitation for all-
external-compression inlets has been computed for free-stream Mach num-
bers from 2.0 to 6.0. Details of the relations used in the calculation
of the compression limits are outlined in the appendix. In figure 15,
a comparison is made between the total-pressure recoveries corresponding
to the compression limit and current experimental maximum recoveries ob-
tained from a survey of the existing literature (refs. 1, 5, 6, and 7).
For the theoretical calculations of this limit, it was assumed that the
flow was compressed isentropically after an initial tip shock (total-
pressure recovery, 0.99) to a static pressure equal to that behind a
normal shock at free-stream Mach number and then followed by a normal
shock located at the entrance to the diffuser (the cowl-lip station).
This process is schematically illustrated by the insert sketch of the
shock pattern shown on figure 15. Frictional or subsonic diffuser losses
were not included in the calculations. At a free-stream Mach number of
approximately 2.2, this limitation first came into effect. The theoreti-
cal maximum recovery then fell off quite rapidly with increasing Mach
number and at the same time crossed over lines of constant kinetic energy
efficiency $\eta_{K.E.}$ as shown on the figure.

This empirical limitation satisfactorily predicted the general shape
and slope of the experimental curve shown in figure 15. The displacement
between the two curves is, for the most part, assignable to the frictional
or subsonic diffuser losses which the calculation did not take into ac-
count. For Mach numbers from 3.0 to 5.6, this difference between the
limiting values and the current experimental maxima was approximately
0.15.

The variation of the final Mach number limit with free-stream Mach
number is presented in figure 16. Below Mach number 2.2, this compression
limitation does not exist; however, above this value the final Mach num-
ber limit increases almost linearly. At $M_0 = 6.0$ this final Mach num-
ber limit is equal to 3.0.

3320

CONCLUDING REMARKS

It has, thus, been observed that the performance capabilities of high Mach number nose inlets employing conventional all-external-compression surfaces may be limited to levels much lower than heretofore believed possible. With conventional design, then, any future gains in over-all inlet-pressure recovery are apt to be small and come from the direction of improved boundary-layer control and improved subsonic diffusion. On the other hand, there may be some promise in the use of different design procedures such as the utilization of internal contraction with adequate boundary-layer control and means for coping with the initial starting problem (such as perforations or variable geometry.) However, for these a loss in terms of drag or complex mechanisms, again, may more than offset any gains in recovery.

SUMMARY OF RESULTS

An experimental analysis of the compression fields around axially symmetric isentropic spikes with varying degrees of compressive turning was conducted at a Mach number of 3.85. Results were extended to other Mach numbers and are as follows:

1. For all-external-compression inlets above a Mach number of 2.2, there appeared to be a practical design limitation on the degree of compressive flow turning which corresponded to that producing a static-pressure rise equal to that across a free-stream normal shock. Over a wide range of Mach numbers (2.0 to 6.0), this limiting condition satisfactorily predicted the shape and the slope of a curve of current experimental maximum recoveries.

2. At a Mach number of 3.85, the limiting condition corresponded to a final Mach number outside of the boundary layer of 1.95 and a theoretical maximum total-pressure recovery of 0.74. The difference between this and a previously reported inlet-pressure recovery of 0.62 is largely assignable to frictional and subsonic diffuser losses.

3. Isentropic survey-spike configurations which exceeded this limit of compressive turning resulted in a reorientation of the shock structure whereby either a bow wave moved out forward of the main shock intersection, or a double-intersection solution was formed with a subsonic expansion field occurring between the two.

Lewis Flight Propulsion Laboratory
    National Advisory Committee for Aeronautics
        Cleveland, Ohio June 23, 1954

APPENDIX - CALCULATION OF COMPRESSION LIMITS

Details of the calculations used in the determination of compression limits as a function of free-stream Mach number are as follows:
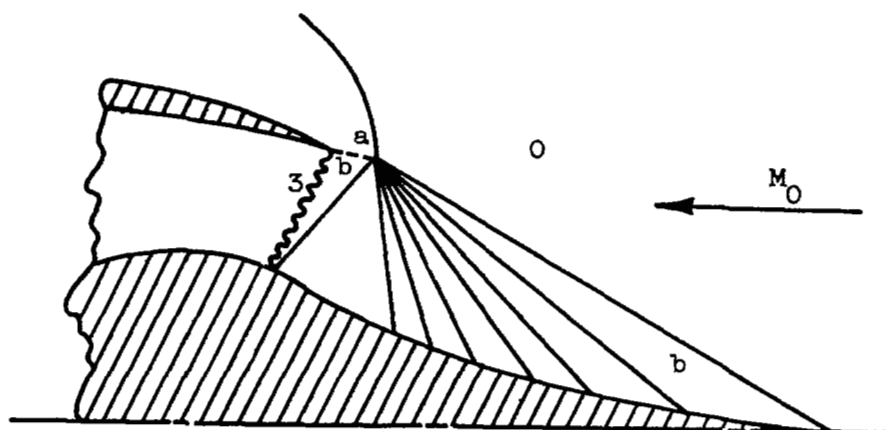
$$M_b = f\left(\frac{p_b}{P_b} = \frac{p_b}{p_0} \quad \frac{p_0}{P_0} \quad \frac{P_0}{P_b}\right)$$

where

$p_b/p_0 = p_a/p_0$ static-pressure ratio across a free-stream normal shock

p_0/P_0 ratio of static to total pressure at free-stream Mach number

P_b/P_0 0.99 (initial shock loss)

$$\frac{P_3}{P_0} = \frac{P_b}{P_0} \quad \frac{P_3}{P_b} \approx (0.99)\frac{P_3}{P_b}$$

where

$\dfrac{P_3}{P_b}$ total-pressure ratio across a normal shock at M_b

REFERENCES

1. Connors, James F., and Woollett, Richard R.: Performance Characteristics of Several Types of Axially Symmetric Nose Inlets at Mach Number 3.85. NACA RM E52I15, 1952.

2. Connors, James F., and Woollett, Richard R.: Force, Moment, and Pressure Characteristics of Several Annular Nose Inlets at Mach Number 3.85. NACA RM E53J09, 1954.

3. Ferri, Antonio: Application of the Method of Characteristics to Supersonic Rotational Flow. NACA Rep. 841, 1946. (Supersedes NACA TN 1135.)

4. Moeckel, W. E.: Approximate Method for Predicting Form and Location of Detached Shock Waves Ahead of Plane or Axially Symmetric Bodies. NACA TN 1921, 1949.

5. Hunczak, Henry R.: Pressure Recovery and Mass-Flow Performance of Four Annular Nose Inlets Operating in Mach Number Region of 3.1 and Reynolds Number Range of Approximately 0.45×10^6 to 2.20×10^6. NACA RM E54A07, 1954.

6. Bernstein, Harry, and Haefeli, Rudolph C.: Performance of Isentropic Nose Inlets at Mach Number of 5.6. NACA RM E54B24, 1954.

7. Anon.: Fifth Quarterly Progress Report on Ram Jet Development. Rep. No. 1521, Wright Aeronautical Corp., Apr. 13, 1951. (Contract AF 33(038)-9000.)

TABLE I. - MODEL DIMENSIONS

(a) Isentropic inlet details. A, length of spike from tip to point of attachment to aft body, in; B, length of cowl from lip to point of attachment to outer shell, in.
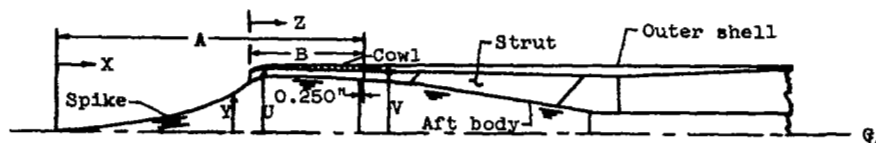
Aft body		Outer shell		
X	Y	Z	U	V
A	1.82 Straight taper	B	2.30 Straight taper	2.50 Cylindrical
A + 4.50	1.22 Straight taper	B + 7.186	2.06 1-in.-rad. arc	
A + 9.13	1.00 Straight cylinder	B + 7.625	2.085 Straight taper	
A + 14.25	1.00	B + 12.75	2.375	2.50

Isentropic				
Spike (A, 14.741)			Cowl (B, 7.750)	
X	Y	Z	U	V
0	0	0	2.240	2.240
.500	.075	.025	2.262	2.272
1.000	.145	.050	2.277	2.291
1.500	.216	.100	2.299	2.323
2.000	.284	.200	2.328	2.370
2.500	.357	.300	2.346	2.404
3.000	.436	.400	2.358	2.432
3.500	.528	.500	2.370	2.469
4.000	.624	.800	2.376	2.492
4.500	.742	1.000	2.378	2.500
5.000	.876		Cylindrical	Cylindrical
5.500	1.031			
6.000	1.210	5.300	2.378	
6.500	1.433	5.500	2.376	
7.000	1.746	5.750	2.370	
7.100	1.830	6.000	2.360	
7.200	1.922		Straight taper	
7.300	2.025			
7.400	2.100	7.760	2.300	2.500
7.500	2.137			
7.600	2.159			
7.700	2.170			
8.000	2.178			
8.230	2.180			
9.000	2.174			
9.188	2.170			
10.000	2.153			
11.000	2.113			
12.000	2.060			
13.000	1.994			
14.000	1.906			
14.741	1.820			

(b) Isentropic survey spike.
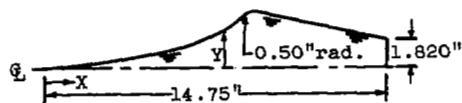
X	Y	X	Y	Design points
1.000	0.143	7.500	1.529	
2.000	.284	7.750	1.636	
3.000	.431	8.000	1.754	
4.000	.590	8.055	1.781	
4.500	.683	8.274	1.898	
5.000	.786	8.450	2.002	F
5.500	.904	8.607	2.108	E
6.000	1.033	8.770	2.232	D
6.500	1.178	8.860	2.315	C
7.000	1.342	8.973	2.437	B
7.250	1.433	9.040	2.516	A
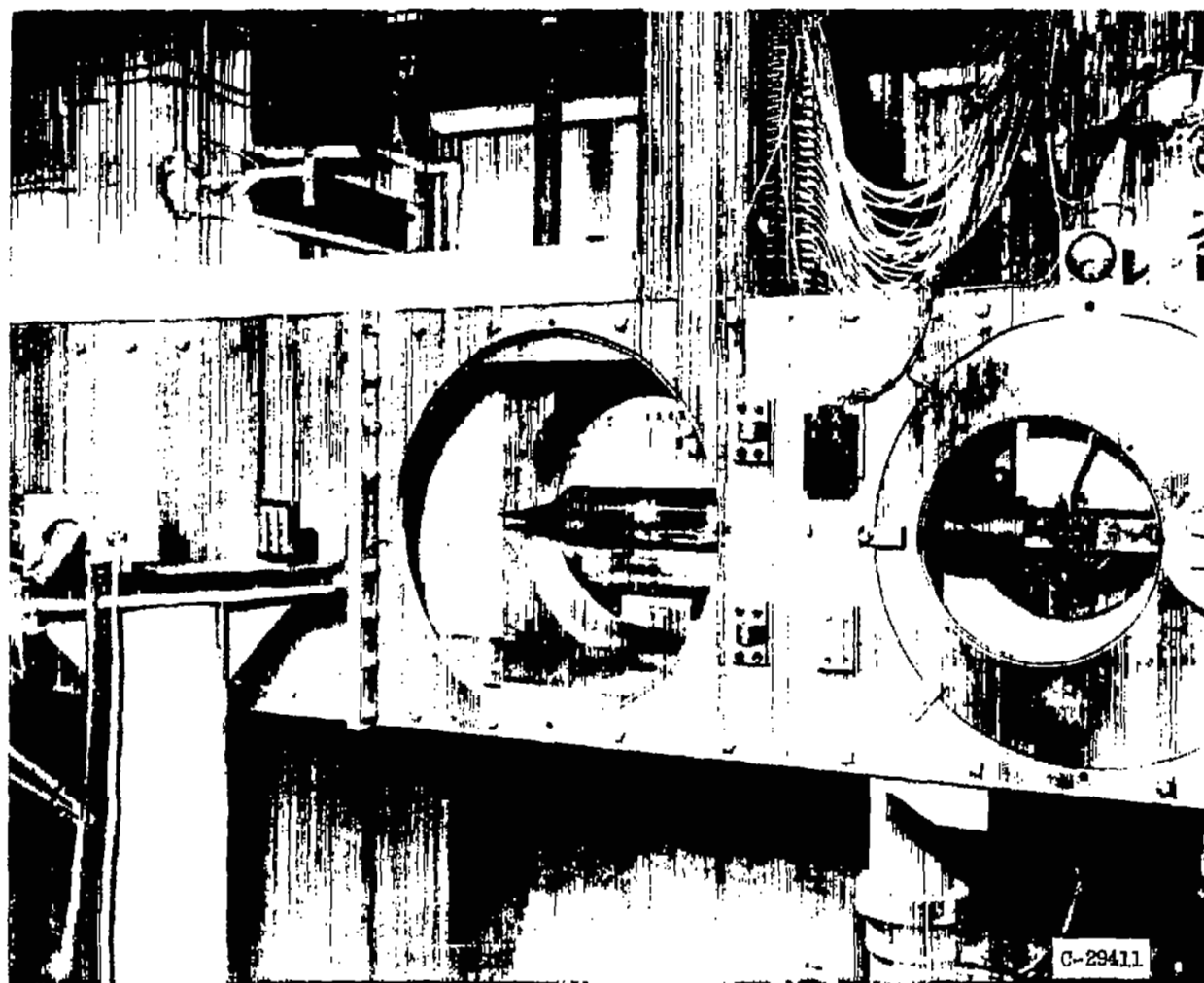
(a) Isentropic inlet installed in 2- by 2-foot supersonic tunnel.

Figure 1. - Experimental apparatus.
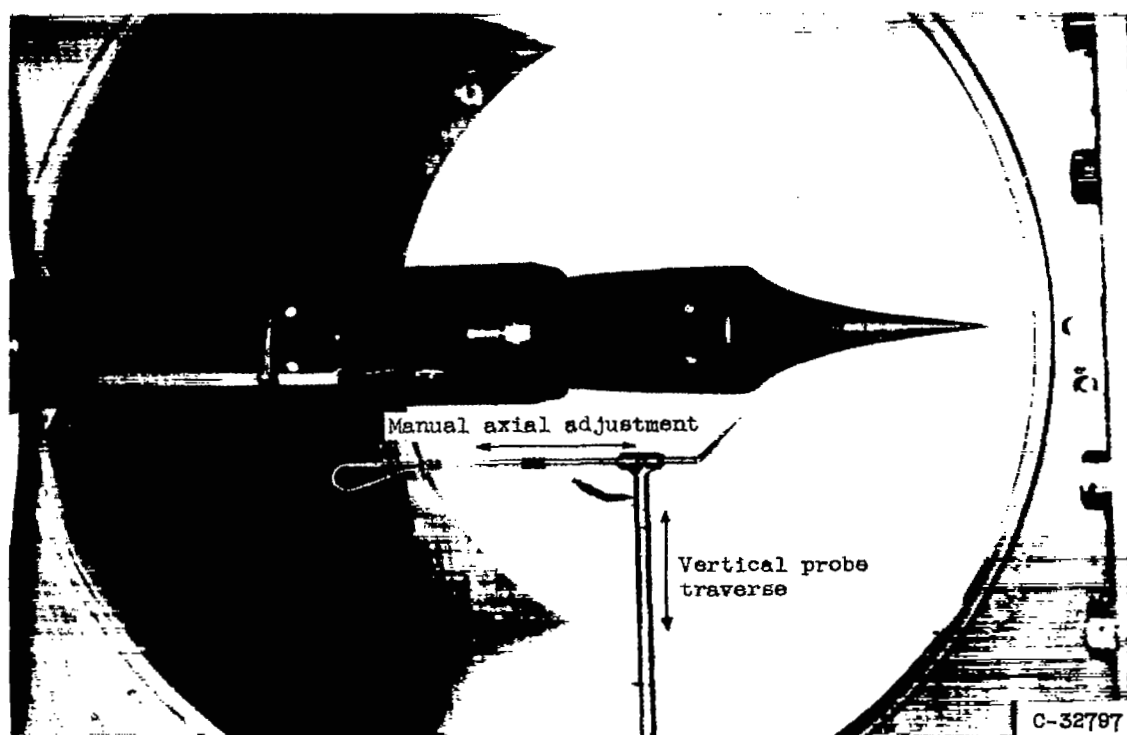
(b) Isentropic spike and pitot-probe survey mechanism in tunnel test section.

0.040"   0.015"   Used only for original spike configuration

0.020"   0.007"   Used on all configurations except F' and
                          original spike configuration

0.016"   0.004   Used with configuration F'

(c) Pitot-probe tip dimensions.

Figure 1. - Continued. Experimental apparatus.
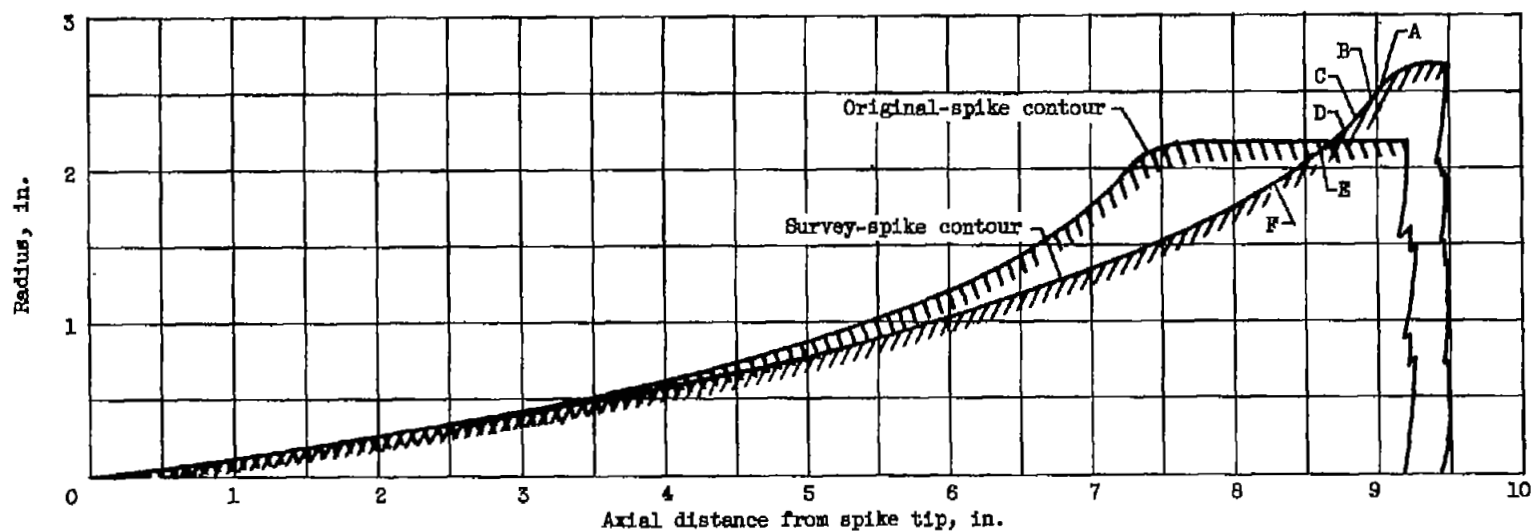
(d) Scale variation between original and survey spikes.

Figure 1. - Continued. Experimental apparatus.
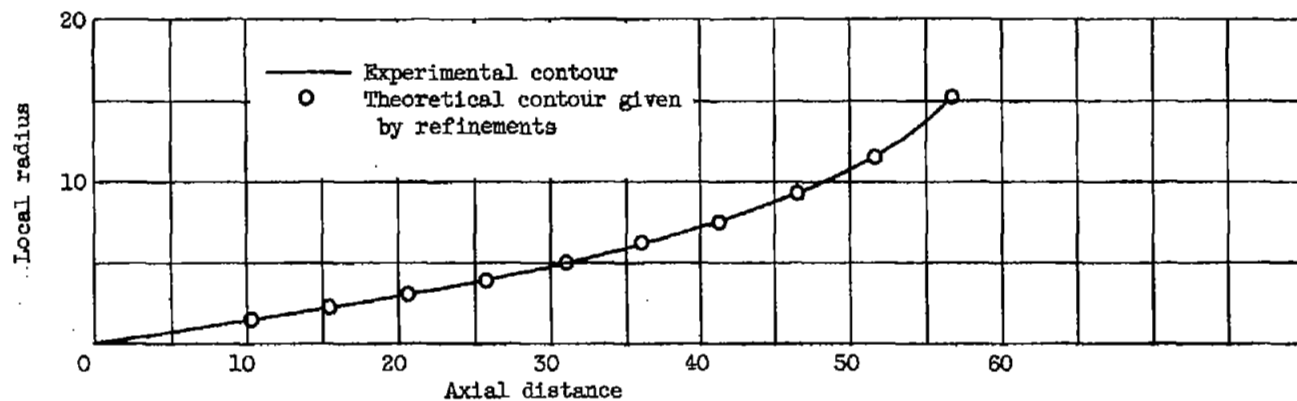
(e) Isentropic spike contours plotted in arbitrary units.
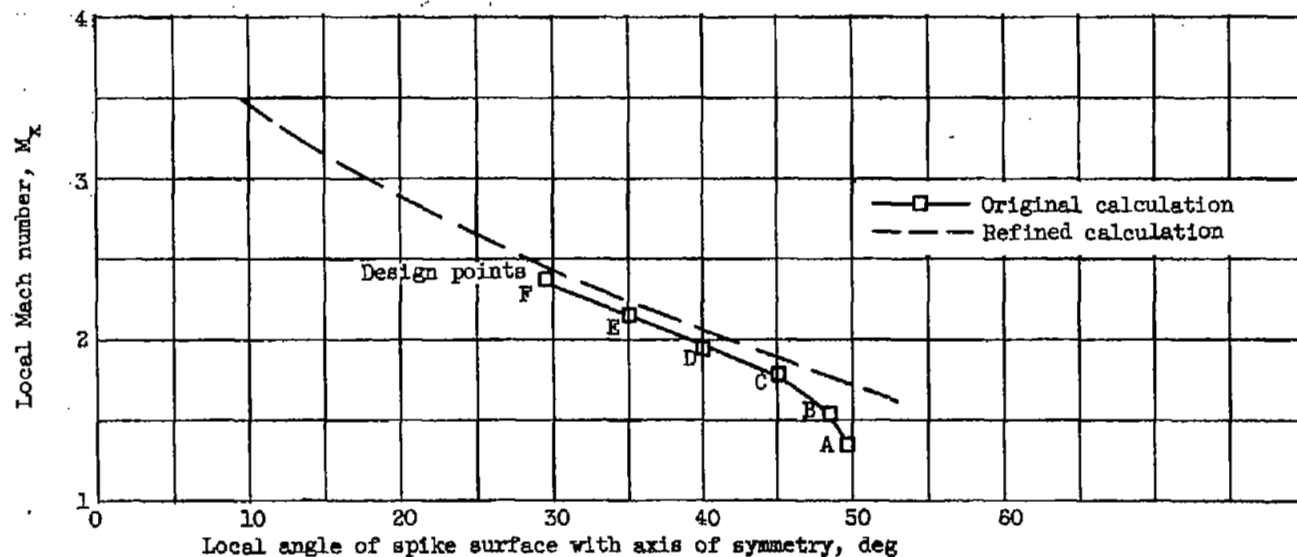
(f) Local Mach number distribution for isentropic spike contours.

Figure 1. - Continued. Experimental apparatus.

Configuration	Theoretical Mach number	Surface angle, deg
A	1.73	49.5
B	1.77	48.5
C	1.89	45.0
D	2.06	40.0
E	2.25	35.0
F	2.45	29.5

Original contour A
Unprimed; immediate expansion; constant radius
Primed; small pressure gradient; conical surface
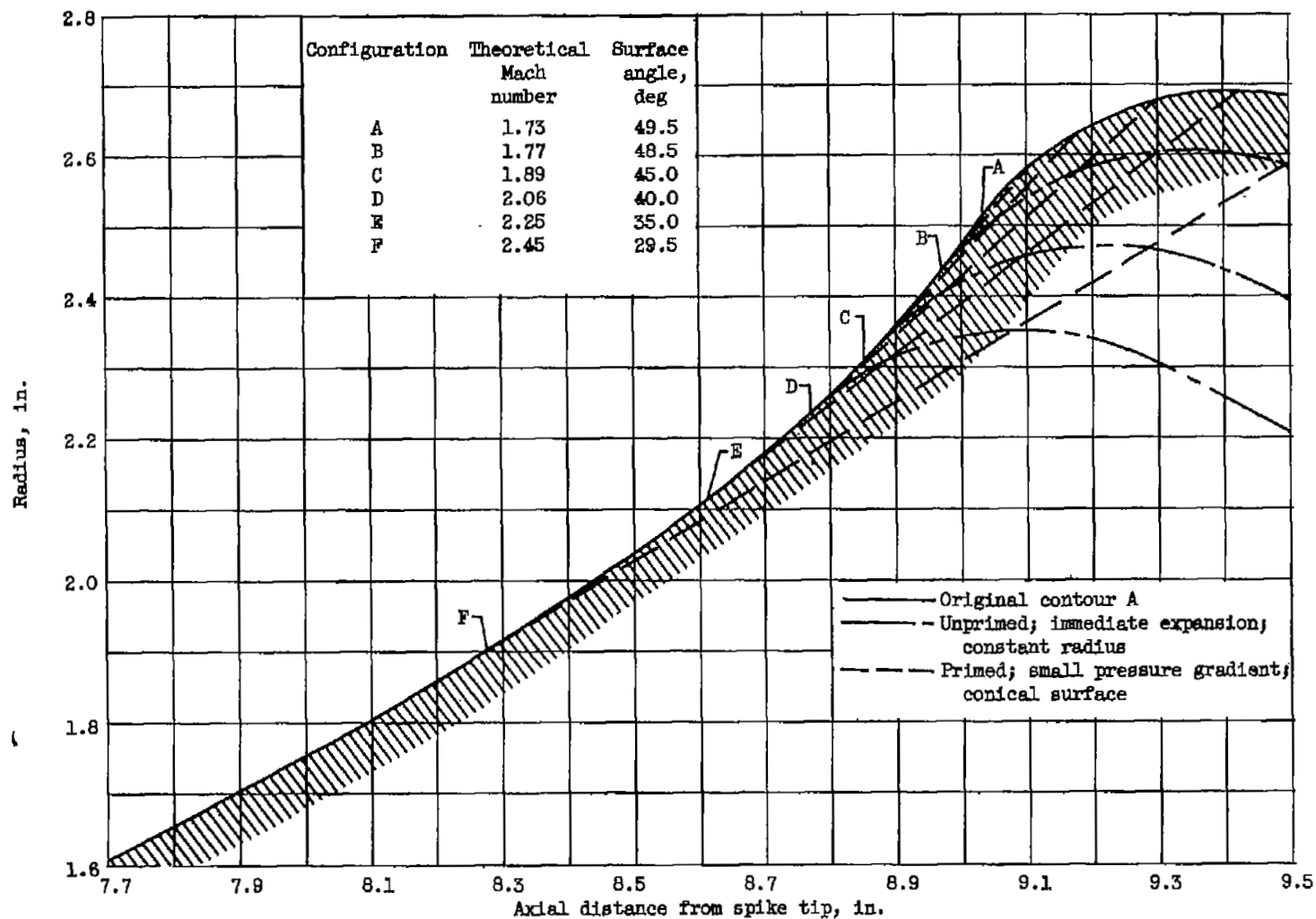
(g) Isentropic survey spike configurations.

Figure 1. - Concluded. Experimental apparatus.
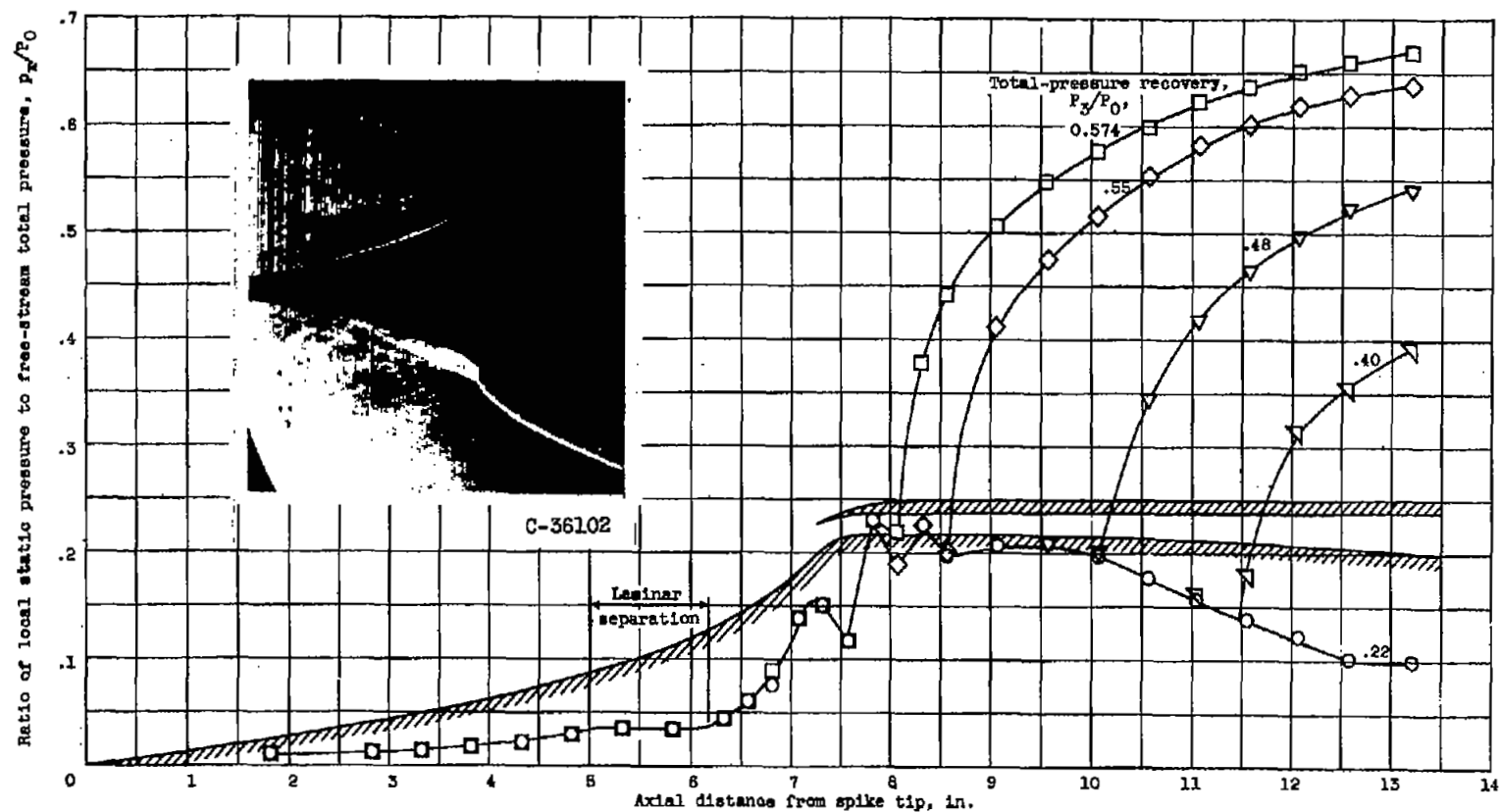
Figure 2. - Static-pressure distributions along spike of isentropic inlet for several supercritical operating conditions. Zero angle of attack and no tip roughness.
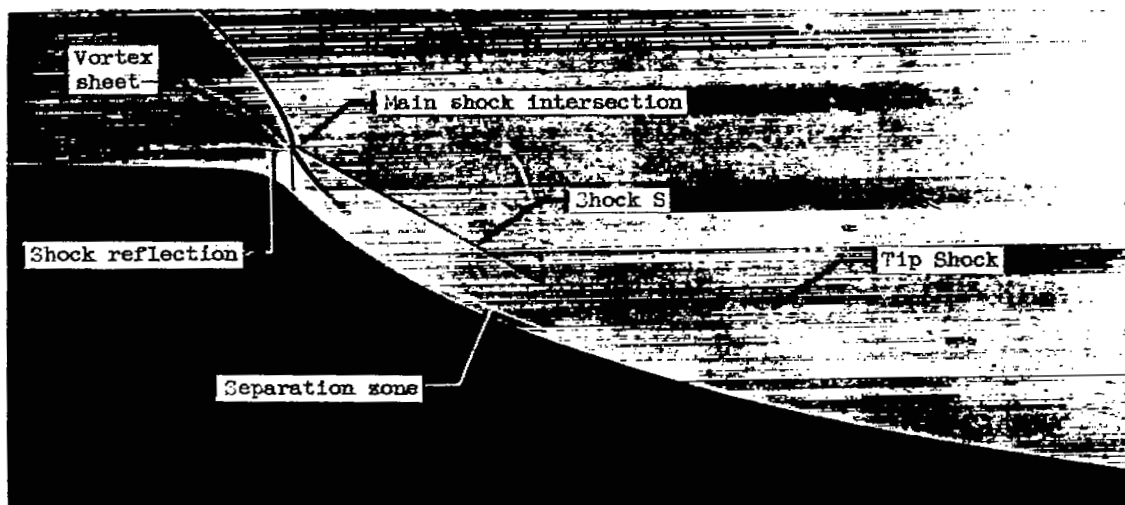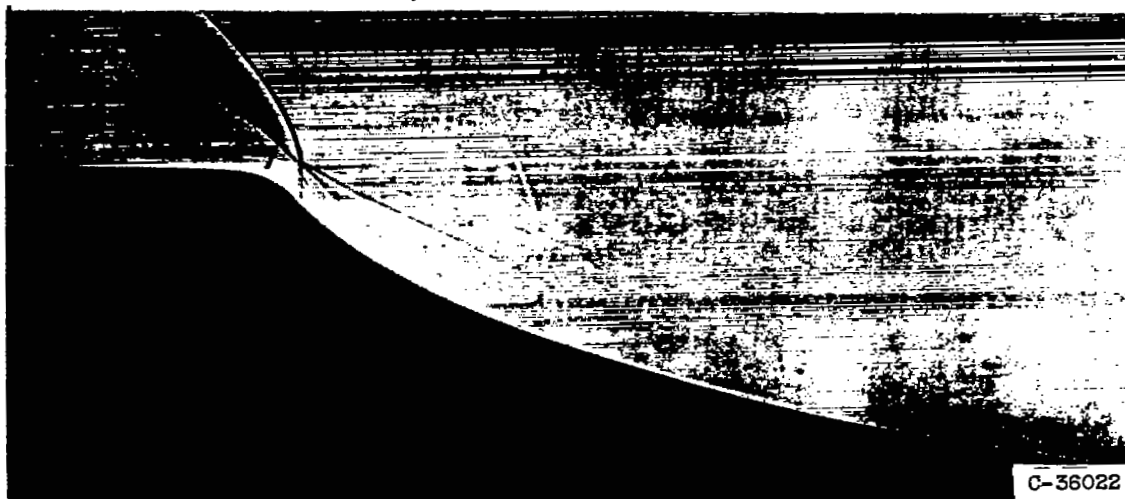
(a) No roughness.

(b) With tip roughness.

Figure 3. - Shadowgraphs of flow patterns obtained with original isentropic spike with inlet-cowl removed.
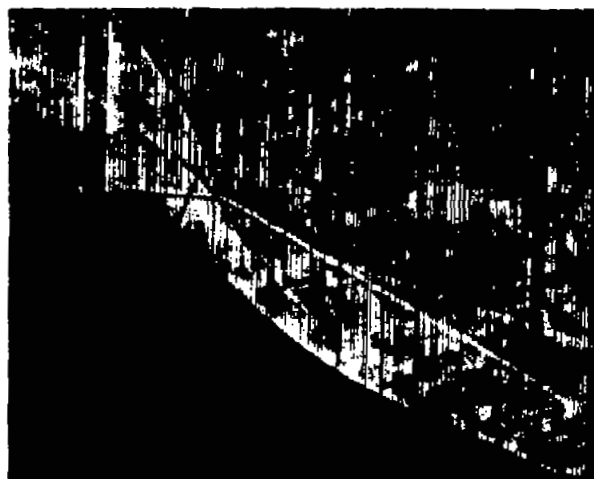
Schlieren   (a) No roughness.   Shadowgraph
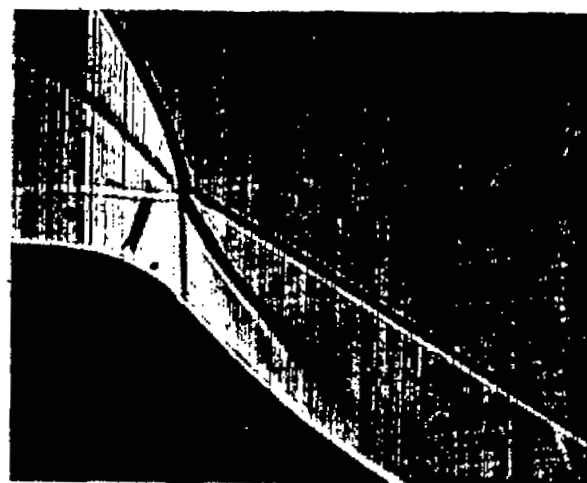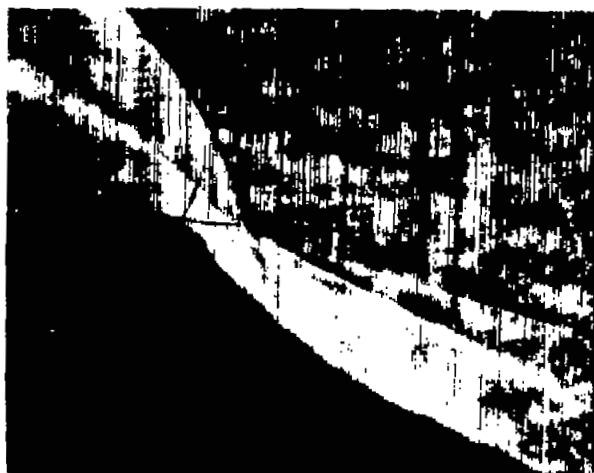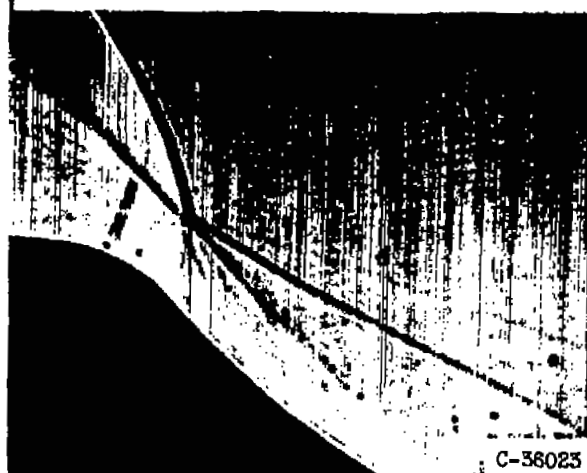
Schlieren   (b) With tip roughness.   Shadowgraph

Figure 4. - Enlarged schlieren photographs and shadowgraphs of flow in vicinity of main shock inter-
section for original isentropic spike.

C-36024
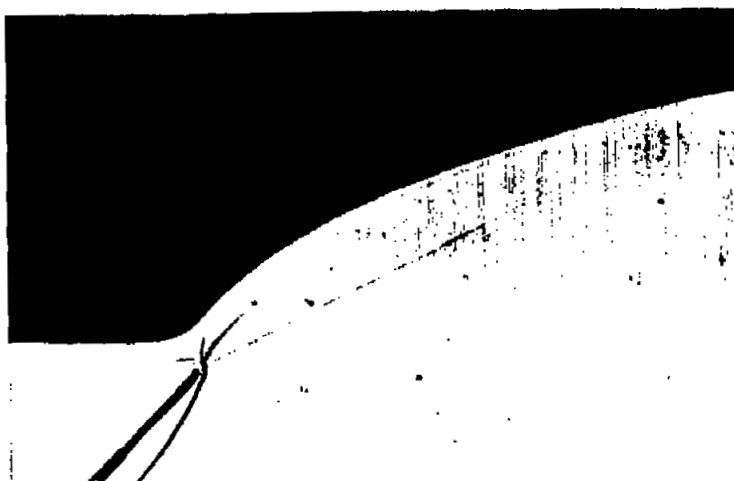
Figure 5. - Typical photographs showing probe in flow field of original isentropic spike.
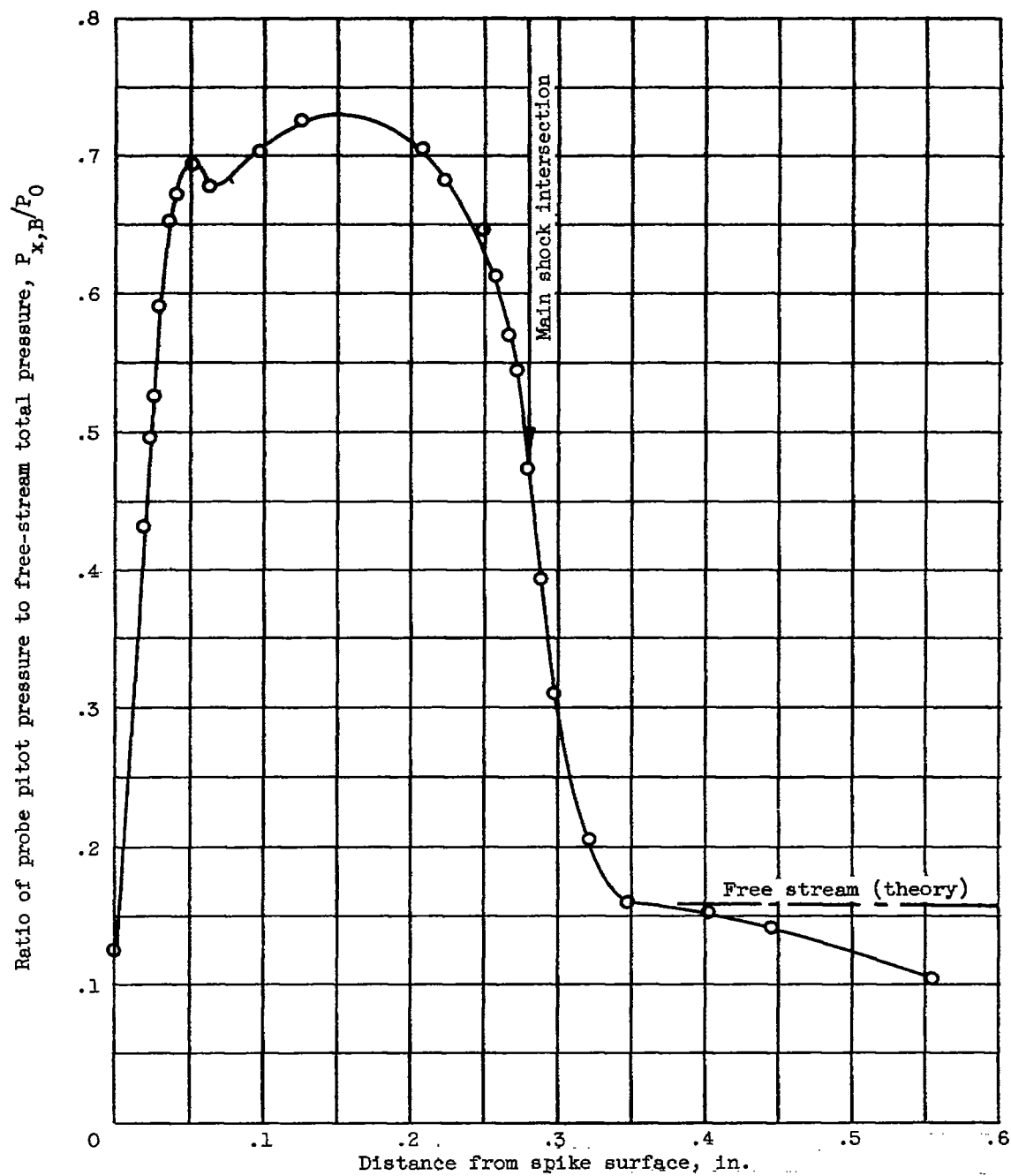
(a) Pitot-pressure profile.

Figure 6. - Profiles of flow in plane of main shock intersection for original isentropic spike.

3320

CN-4 back
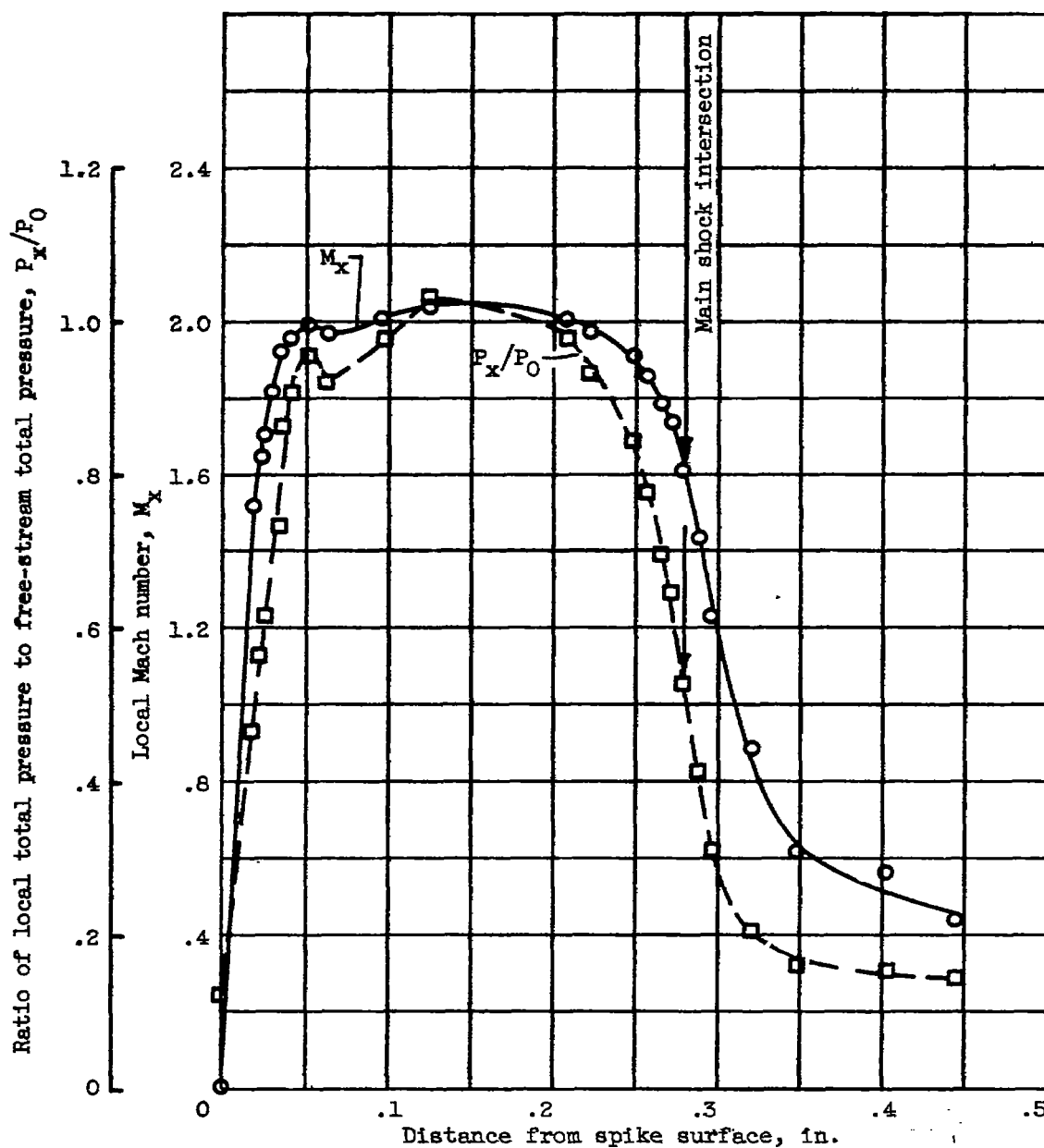
(b) Mach number and total-pressure profiles.

Figure 6. - Concluded. Profiles of flow in plane of main shock intersection for original isentropic spike.
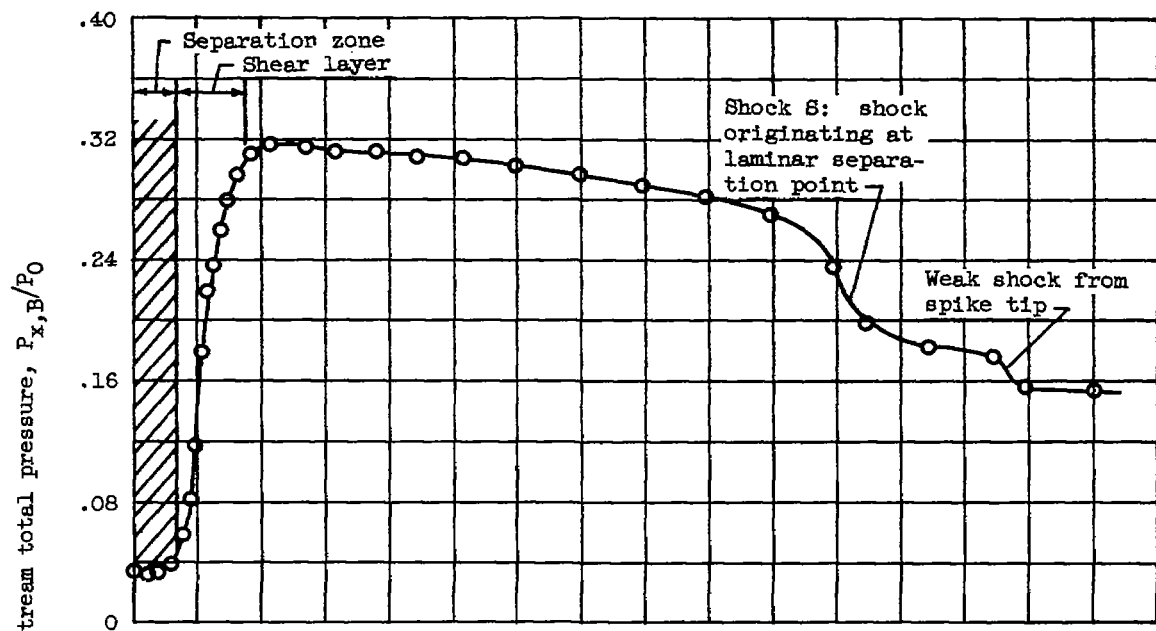
(a) No roughness.
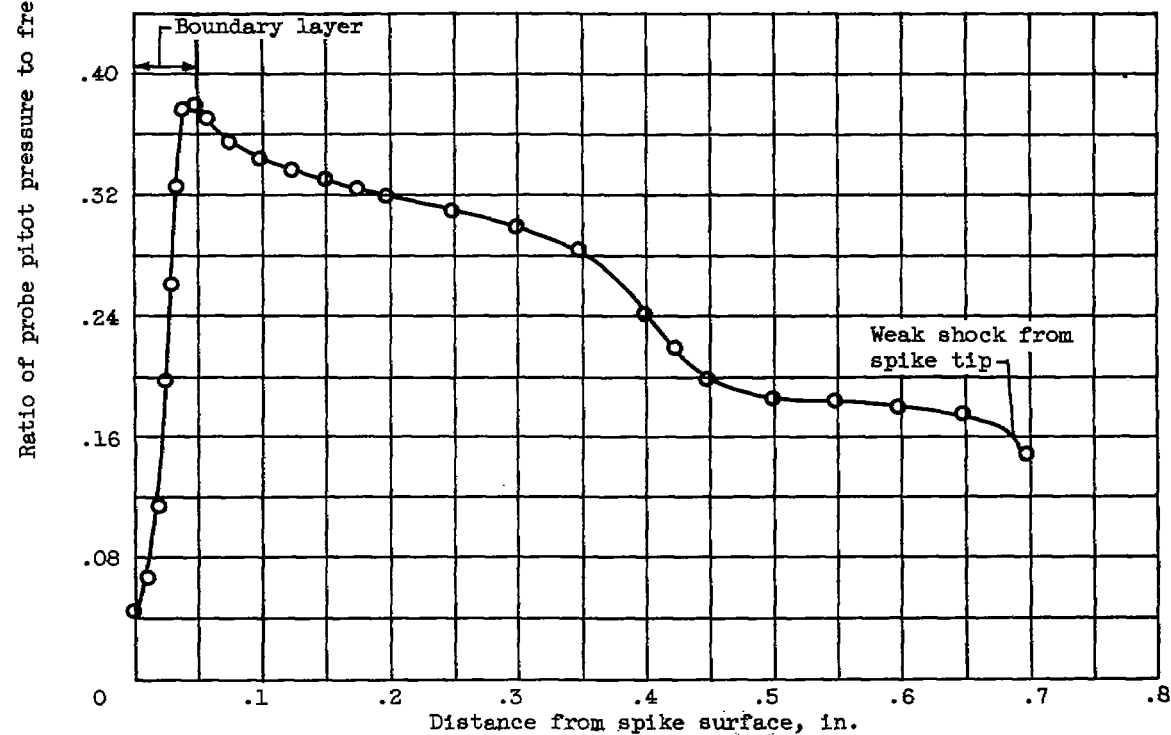
(b) With tip roughness.

Figure 7. - Effect of roughness on boundary layer and main flow field of
original isentropic spike (survey station, 5.8 in. from tip).

Shock S
intersection

Main shock
intersection

No roughness

Main shock
intersection

C-36025
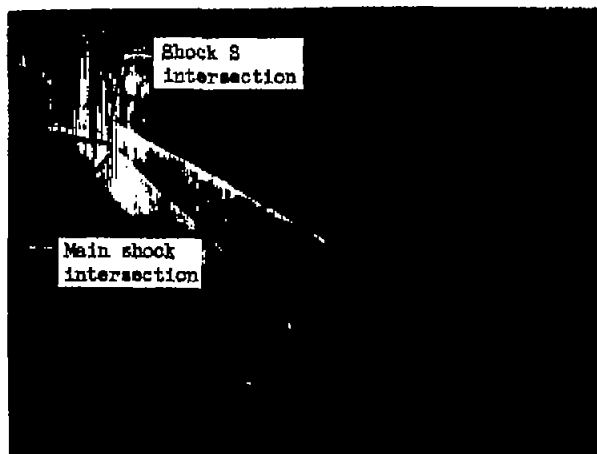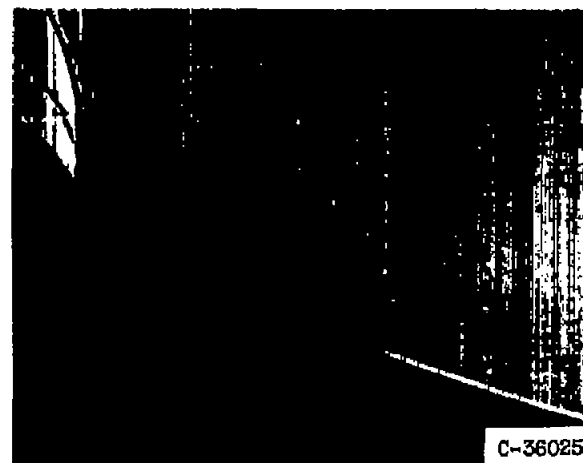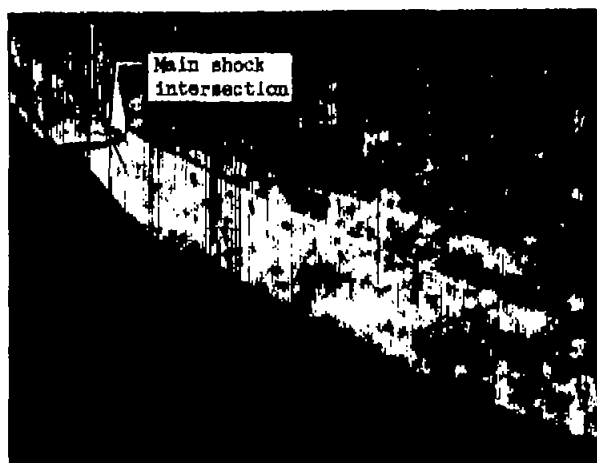
With tip roughness

(a) Configuration A.

Figure 8. - Flow patterns for the various isentropic survey spike configurations.
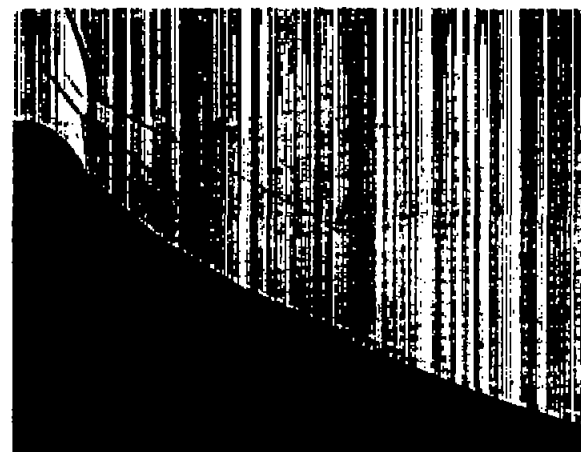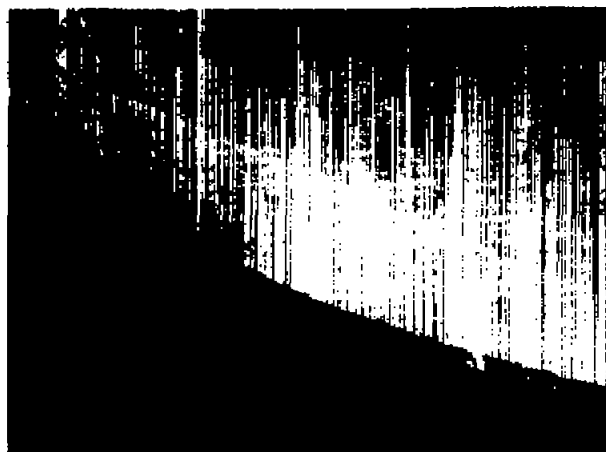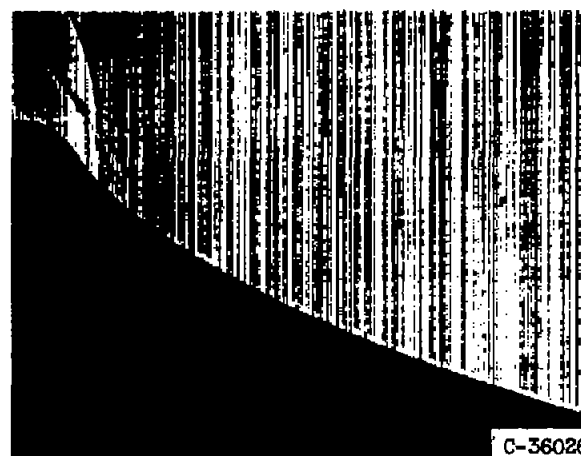
No roughness

With tip roughness

(b) Configuration B'.

Figure 8. - Continued. Flow patterns for various isentropic survey-spike configurations.
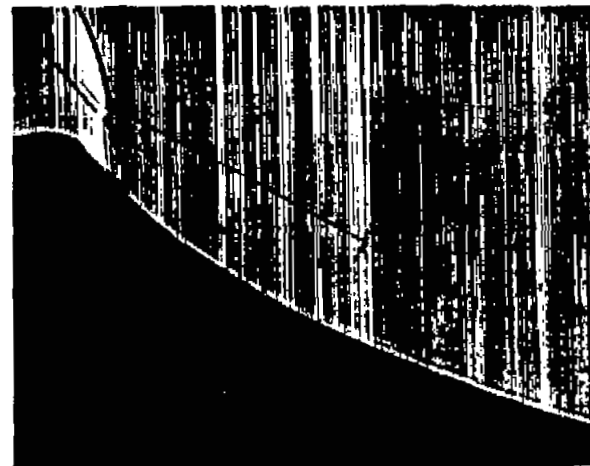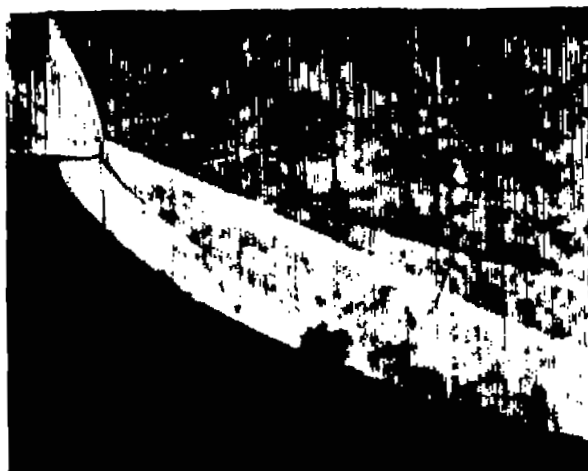
C-36026
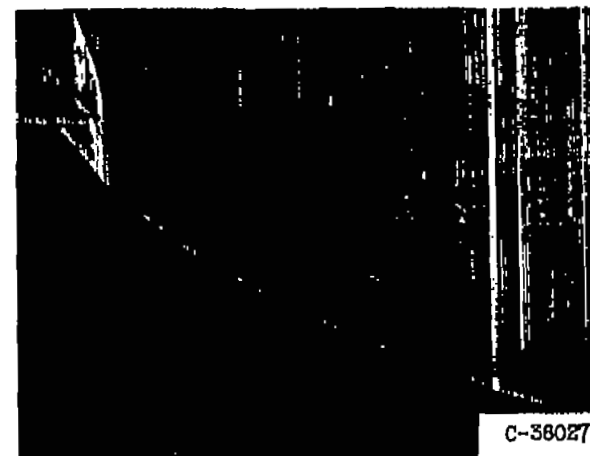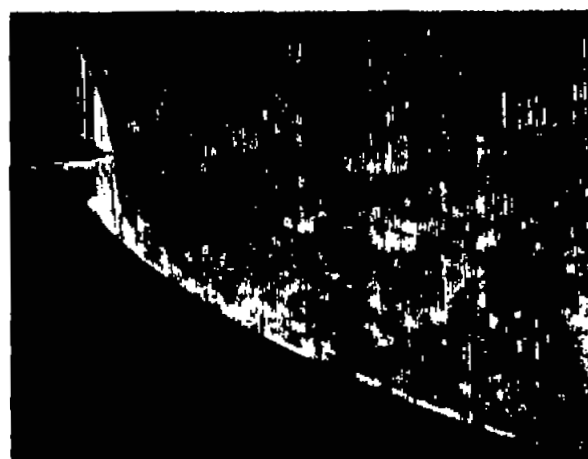
No roughness

With tip roughness

C-36027

(c) Configuration C'.

Figure 8. - Continued. Flow patterns for various isentropic survey-spike configurations.
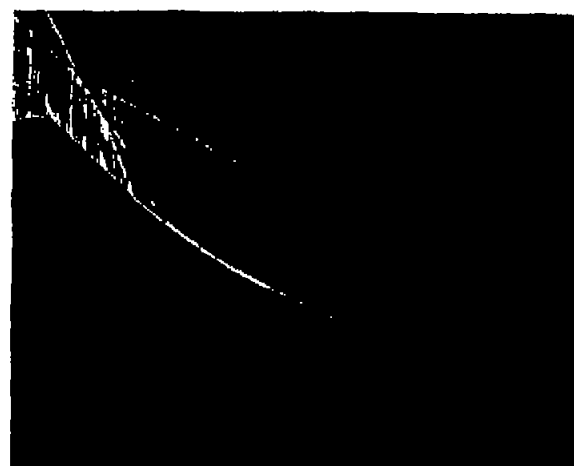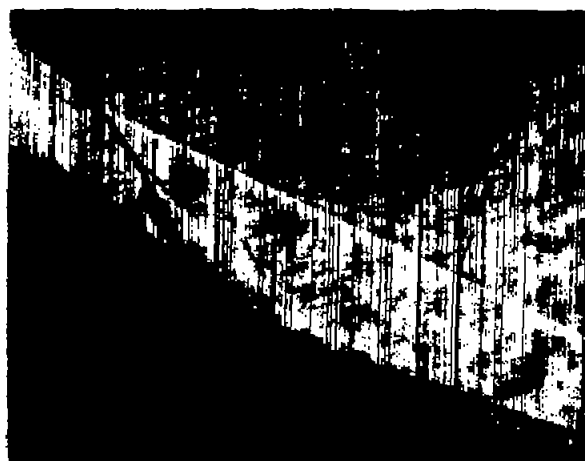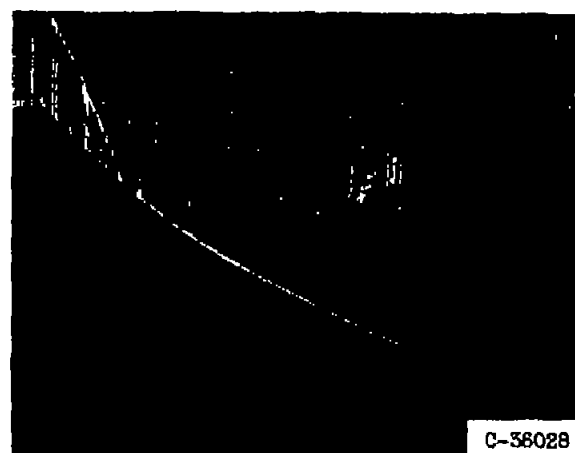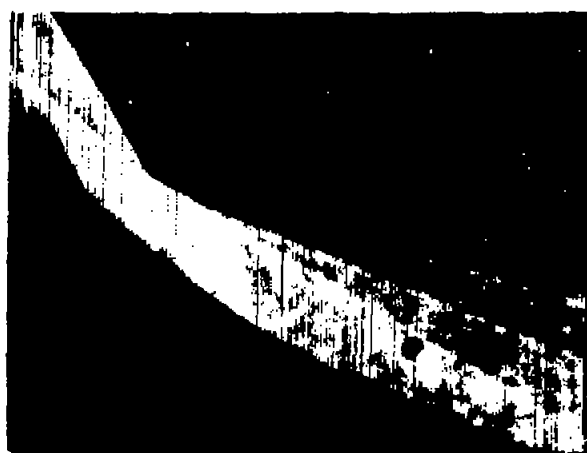
No roughness

With tip roughness

(d) Configuration D'.

Figure 8. - Continued. Flow patterns for various isentropic survey-spike configurations.
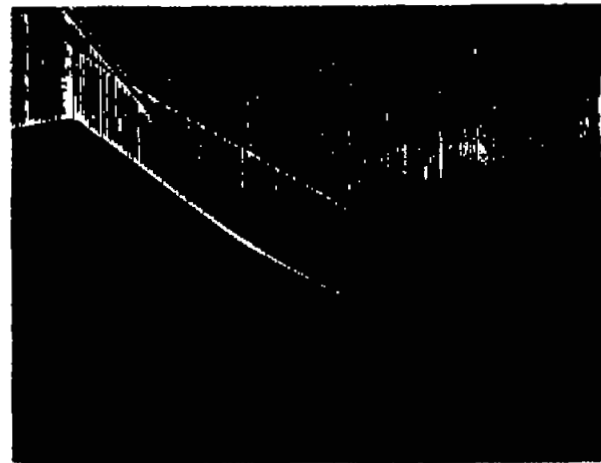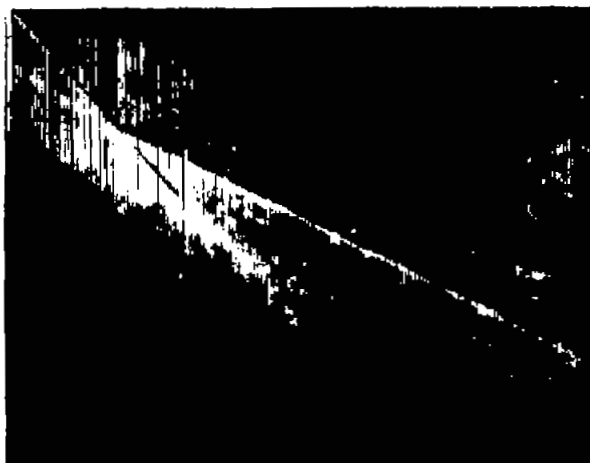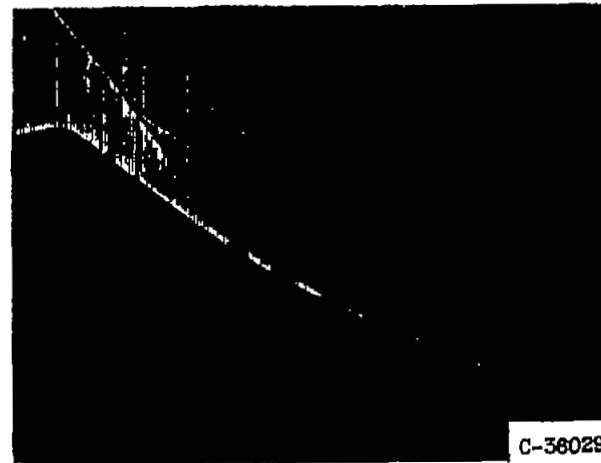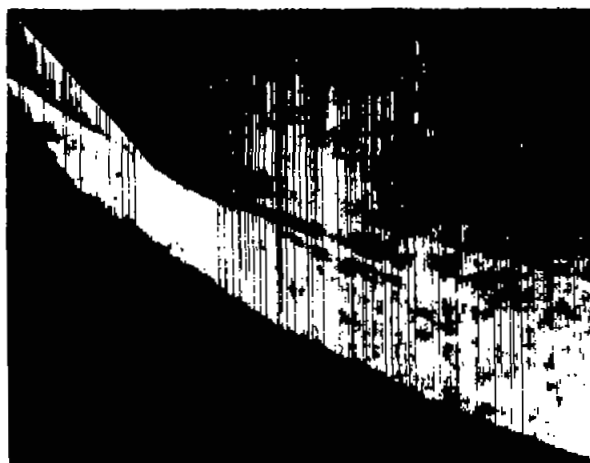
No roughness

With tip roughness

C-36029

(e) Configuration E'.

Figure 8. - Continued. Flow patterns for various isentropic survey-spike configurations.
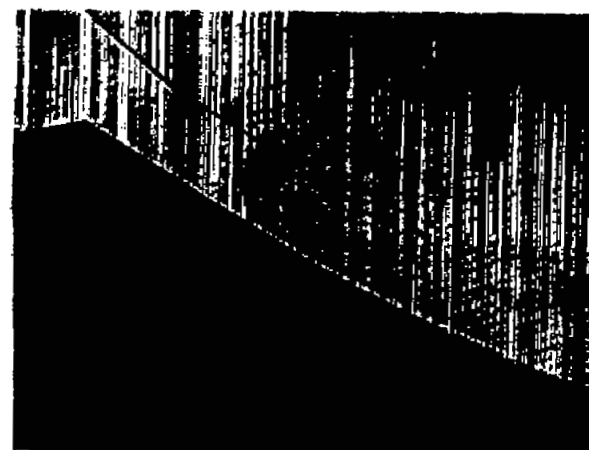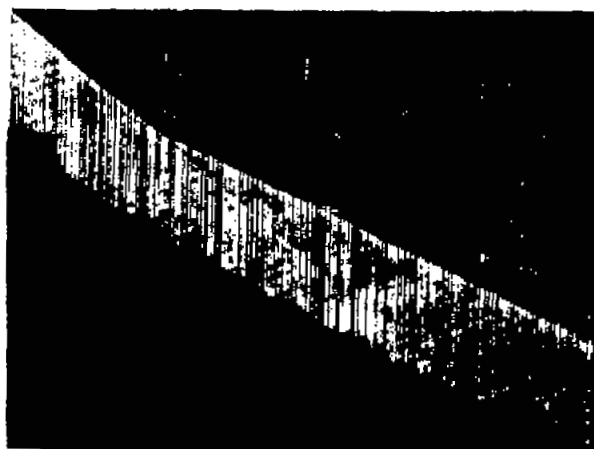
No roughness

With tip roughness

C-36030

(f) Configuration F'.

Figure 8. - Continued. Flow patterns for various isentropic survey-spike configurations.
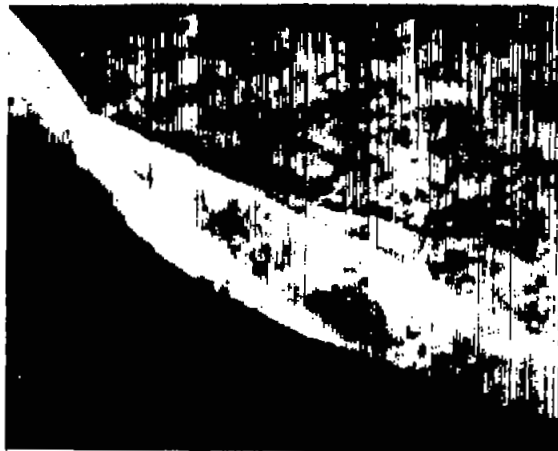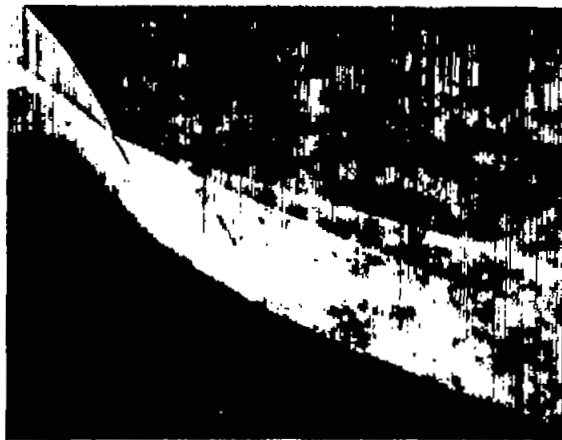
No roughness

With tip roughness   C-36031

(g) Configuration C.

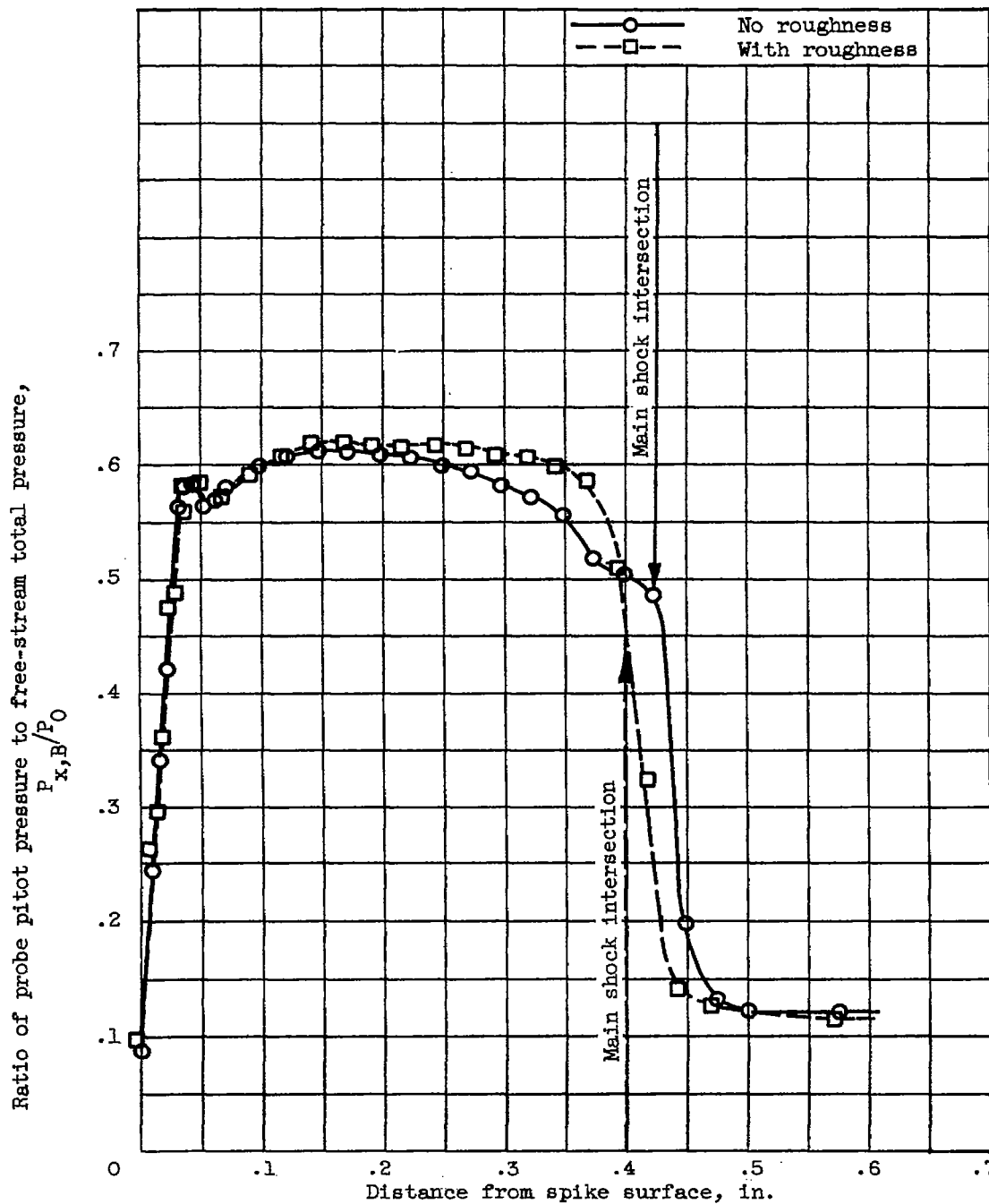Figure 8. - Concluded. Flow patterns for various isentropic survey-spike configurations.
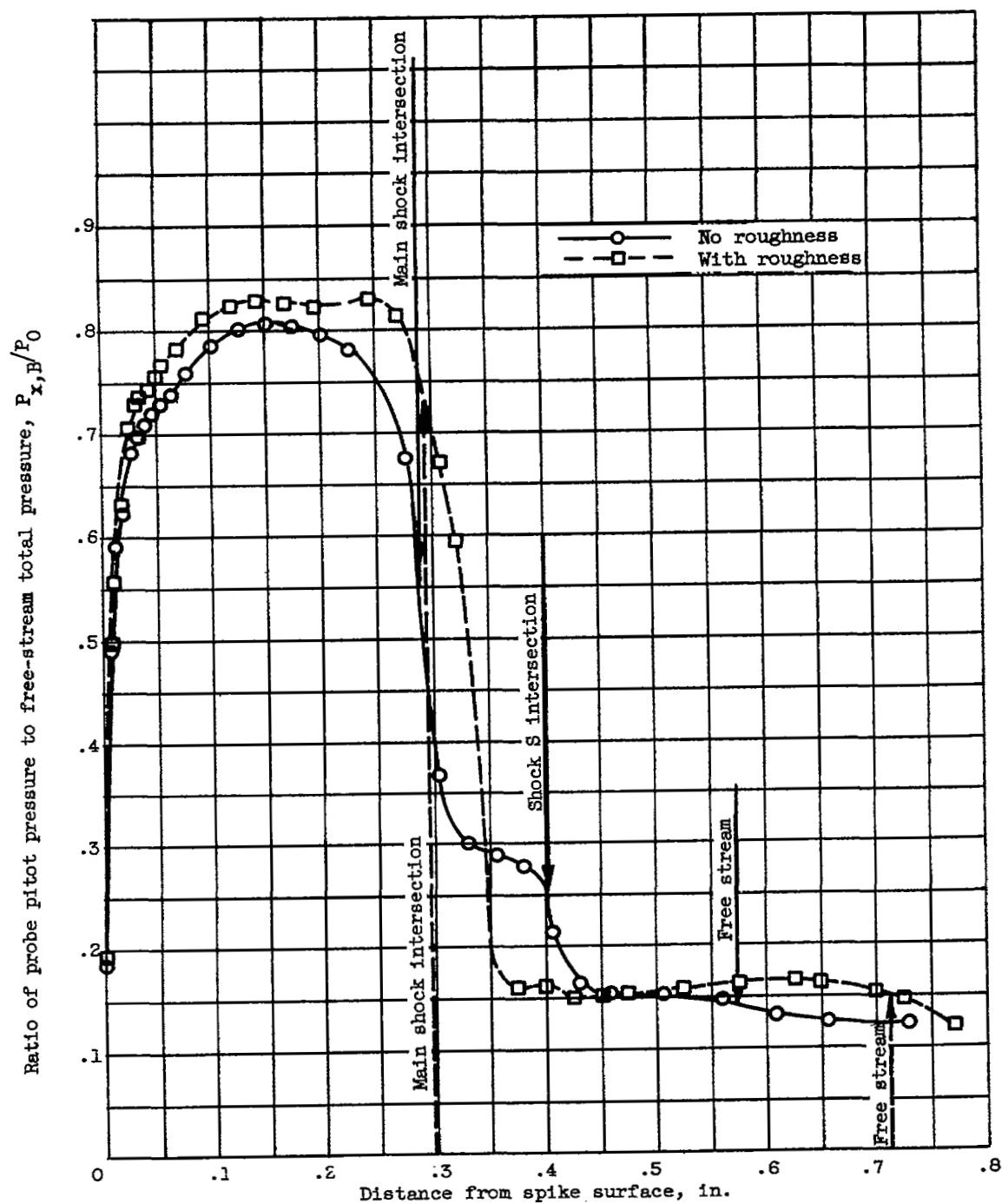
(a) Configurations A and A(R).

Figure 9. - Pitot-pressure profiles of flow in plane of main shock intersection for various isentropic survey-spike configurations.

3320
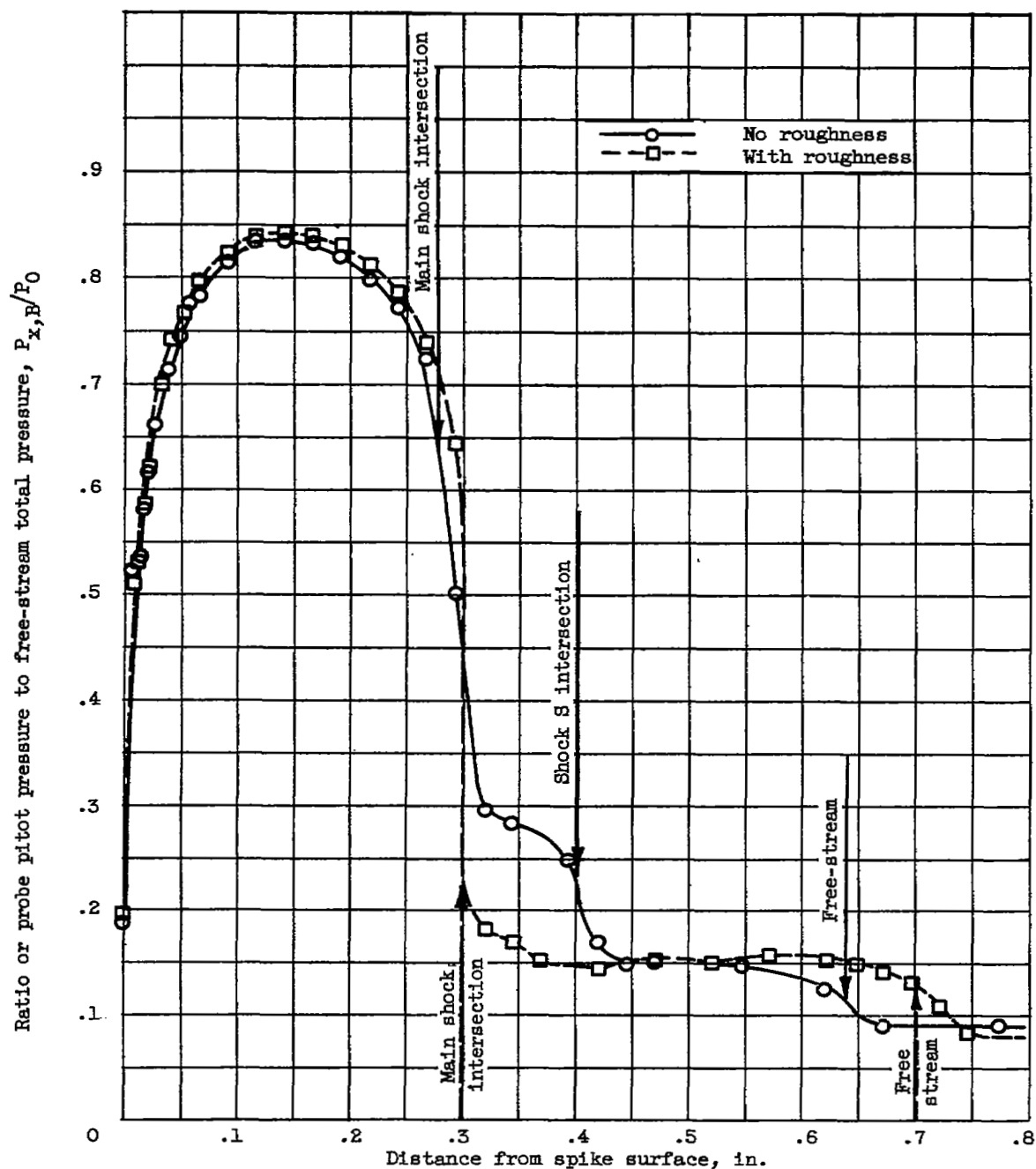
(b) Configurations B' and B'(R).

Figure 9. - Continued. Pitot-pressure profiles of flow in plane of main
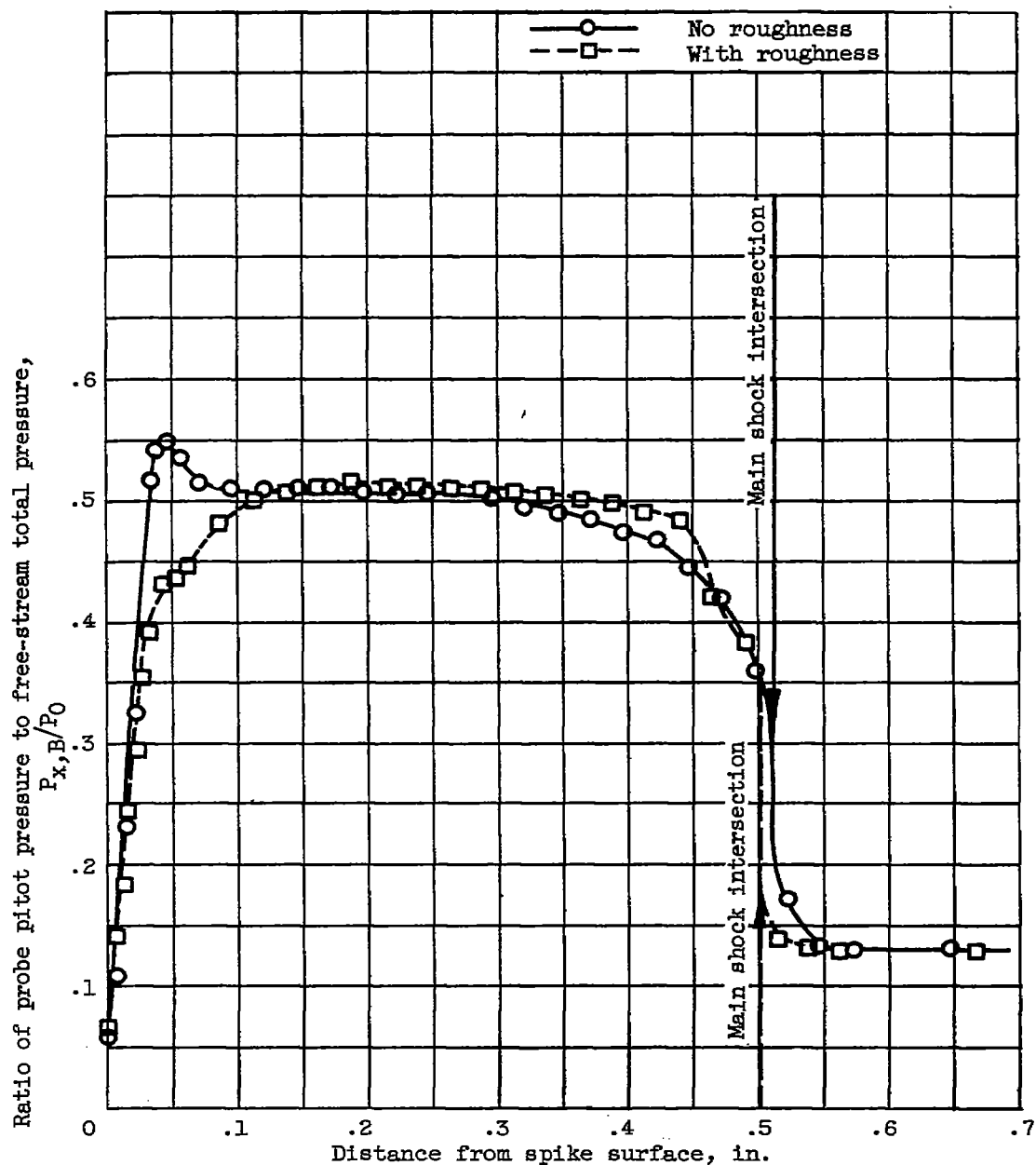shock intersection for various isentropic survey-spike configurations.
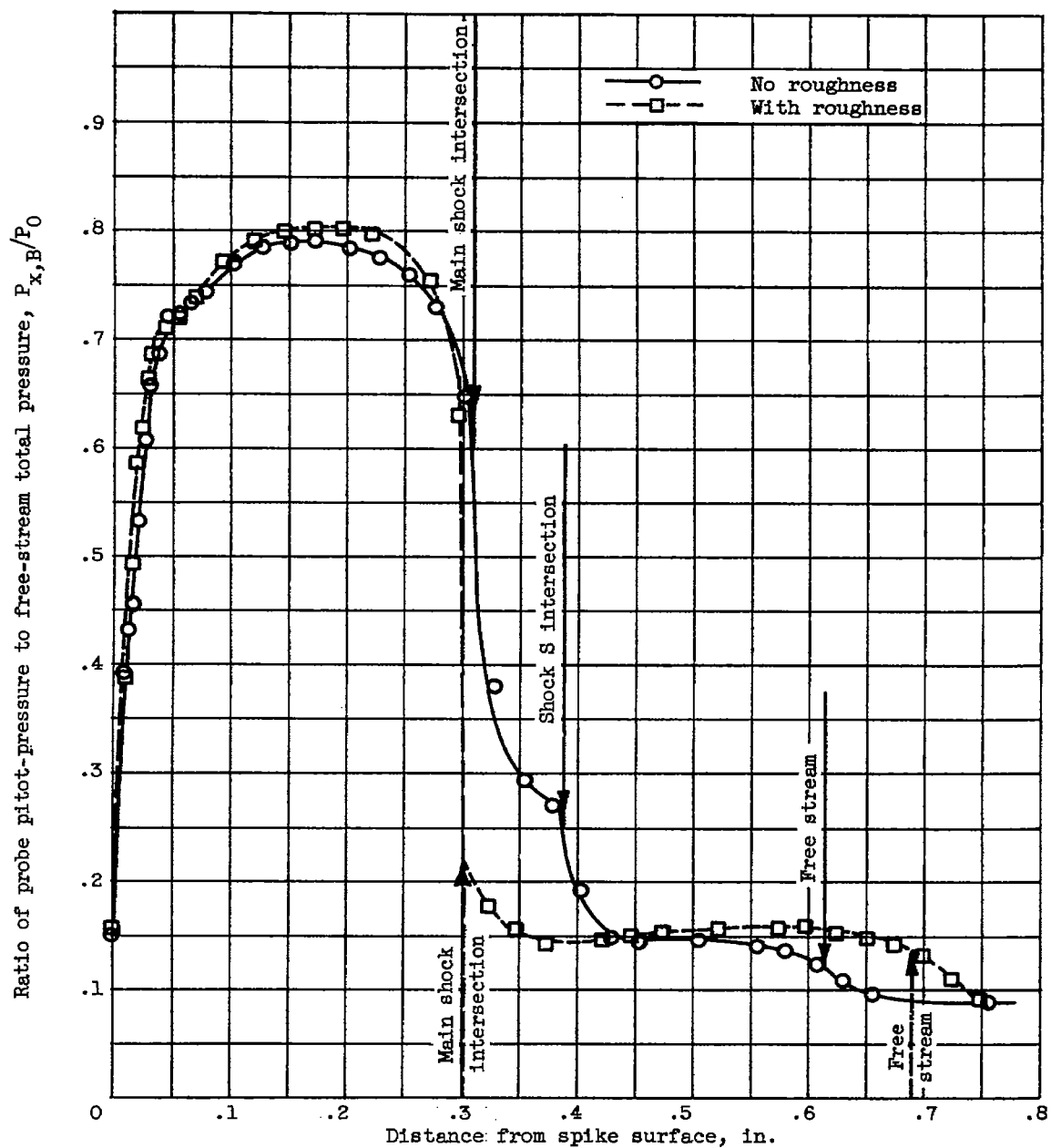
(c) Configurations C' and C'(R).

Figure 9. - Continued. Pitot-pressure profiles of flow in plane of main shock intersection for various isentropic survey-spike configurations.

3320
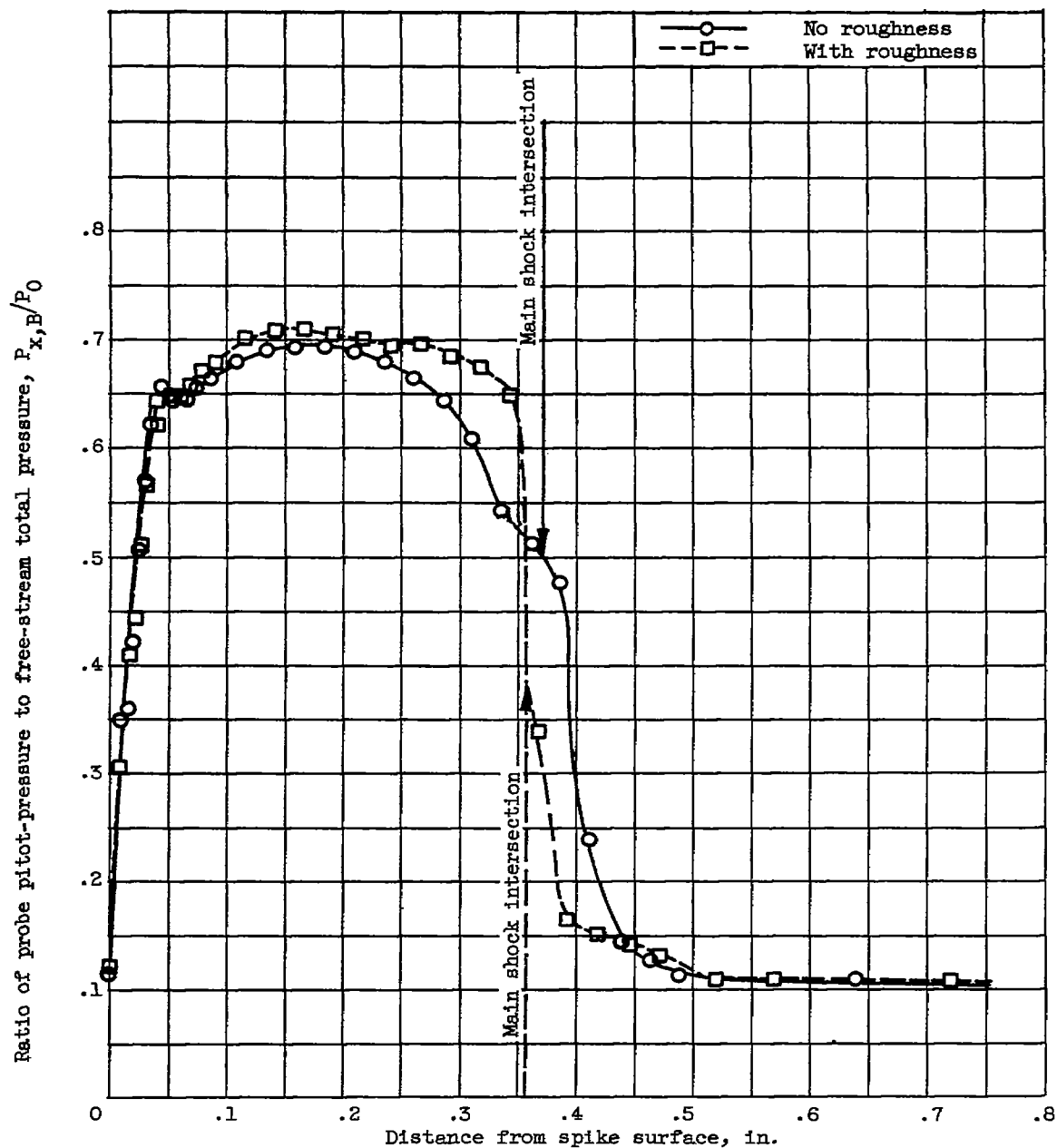
(d) Configurations D' and D'(R).

Figure 9. - Continued. Pitot-pressure profiles of flow in plane of main shock intersection for various isentropic survey-spike configurations.

3320

(e) Configurations E' and E'(R).

Figure 9. - Continued. Pitot-pressure profiles of flow in plane of
main shock intersection for various isentropic survey-spike
configurations.

(f) Configurations F' and F'(R).

Figure 9. - Concluded. Pitot-pressure profiles of flow in plane of
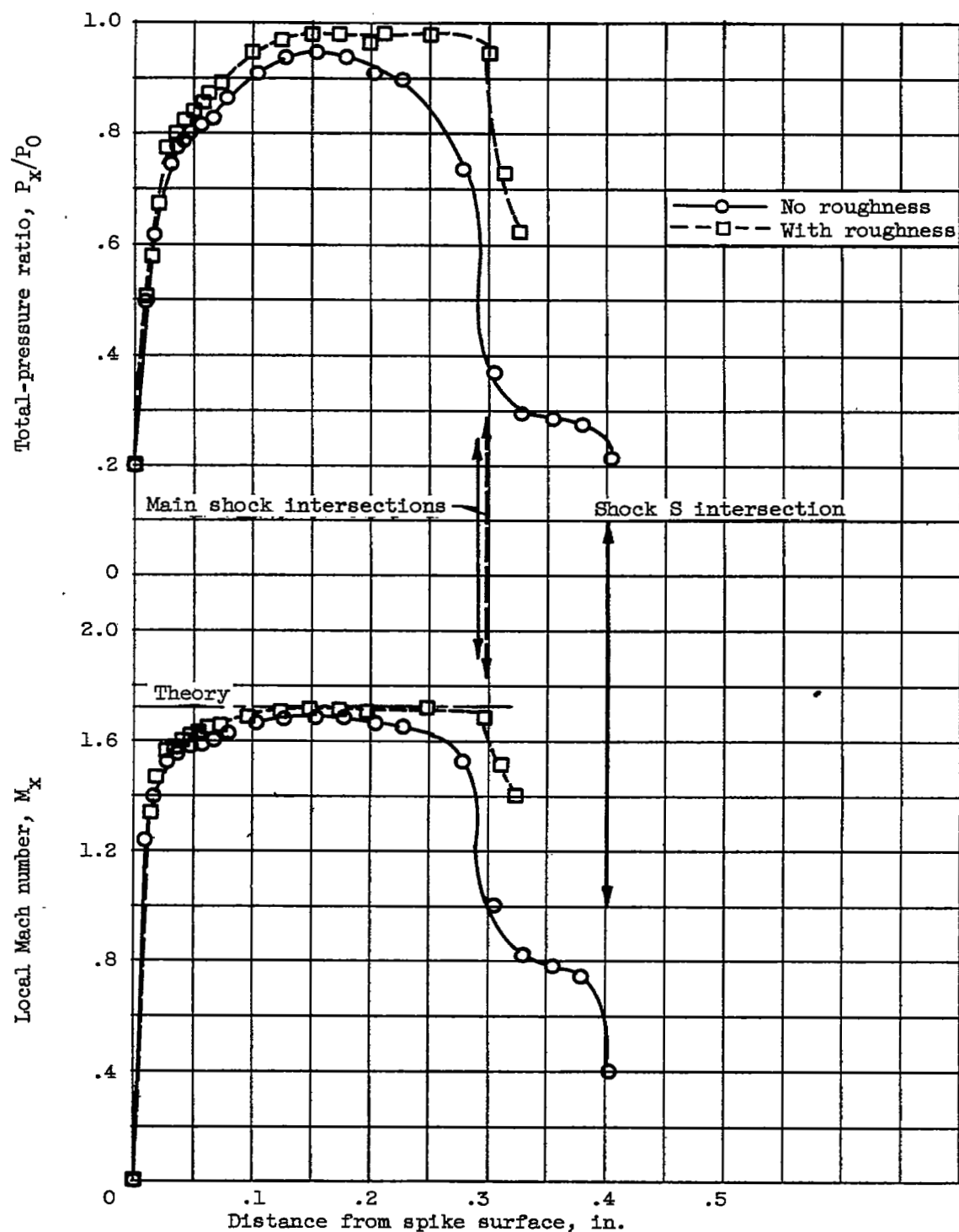main shock intersection for various isentropic survey-spike
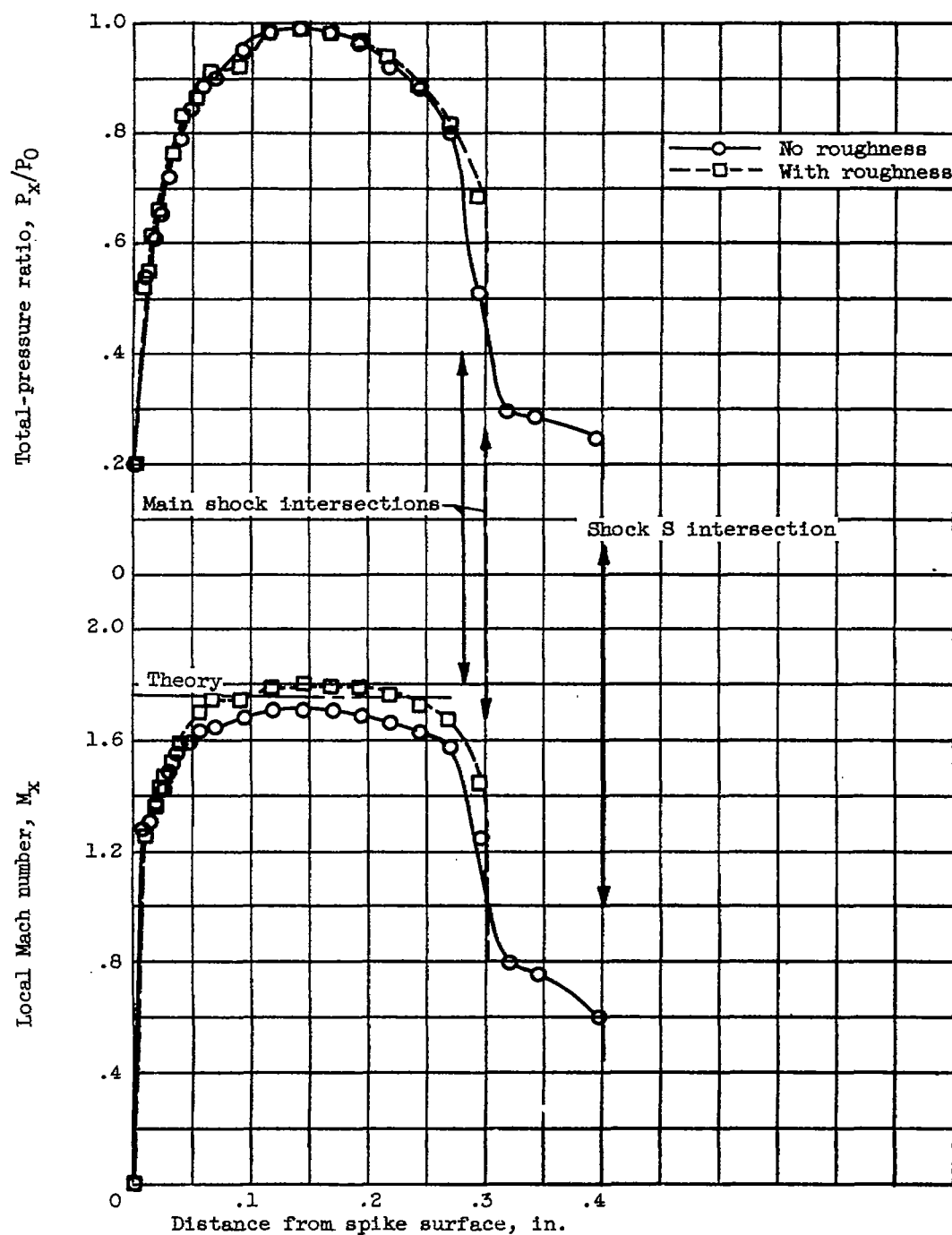configurations.
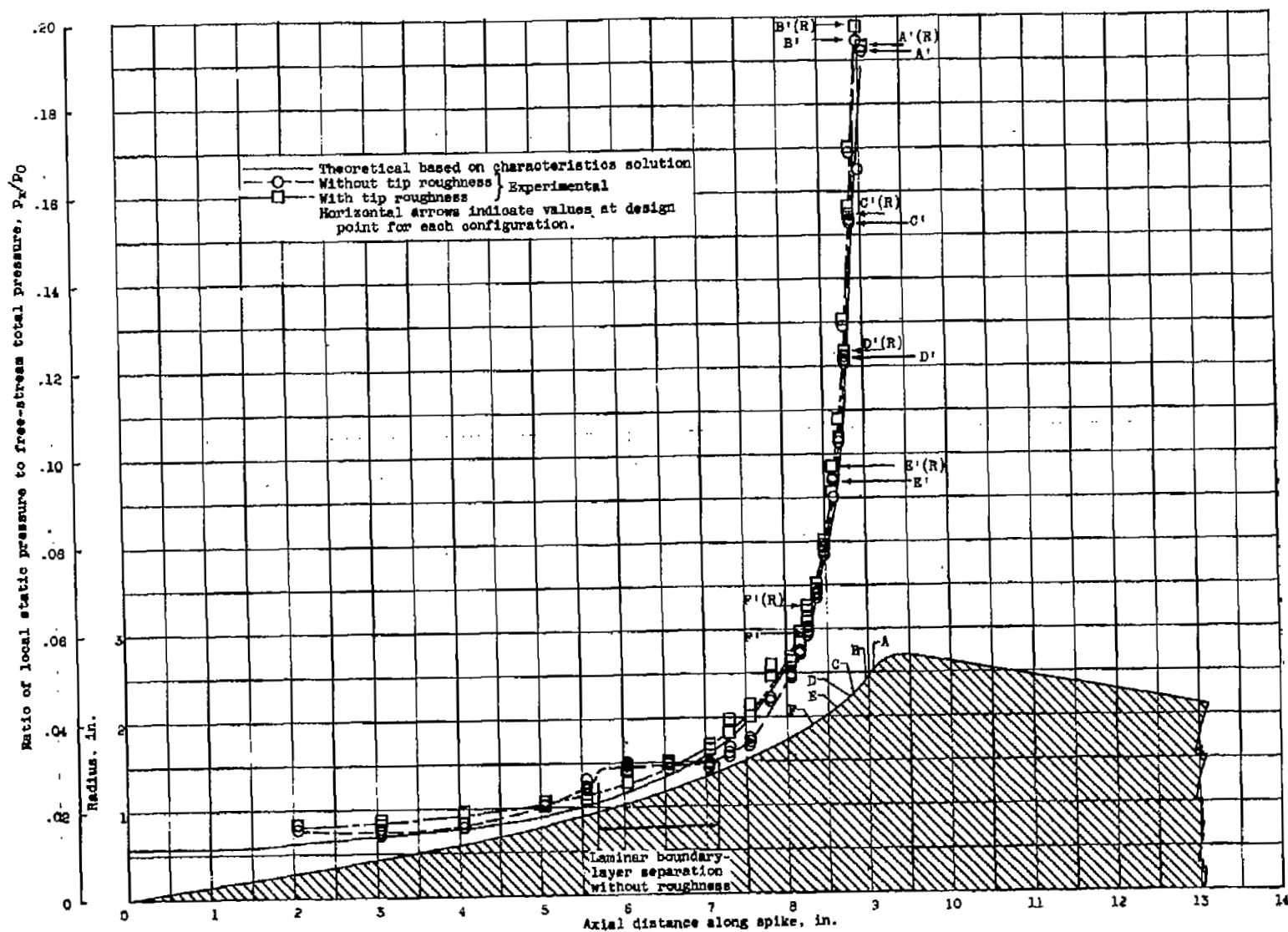
Figure 10. - Static-pressure distributions along surfaces of various isentropic survey-spike configurations.
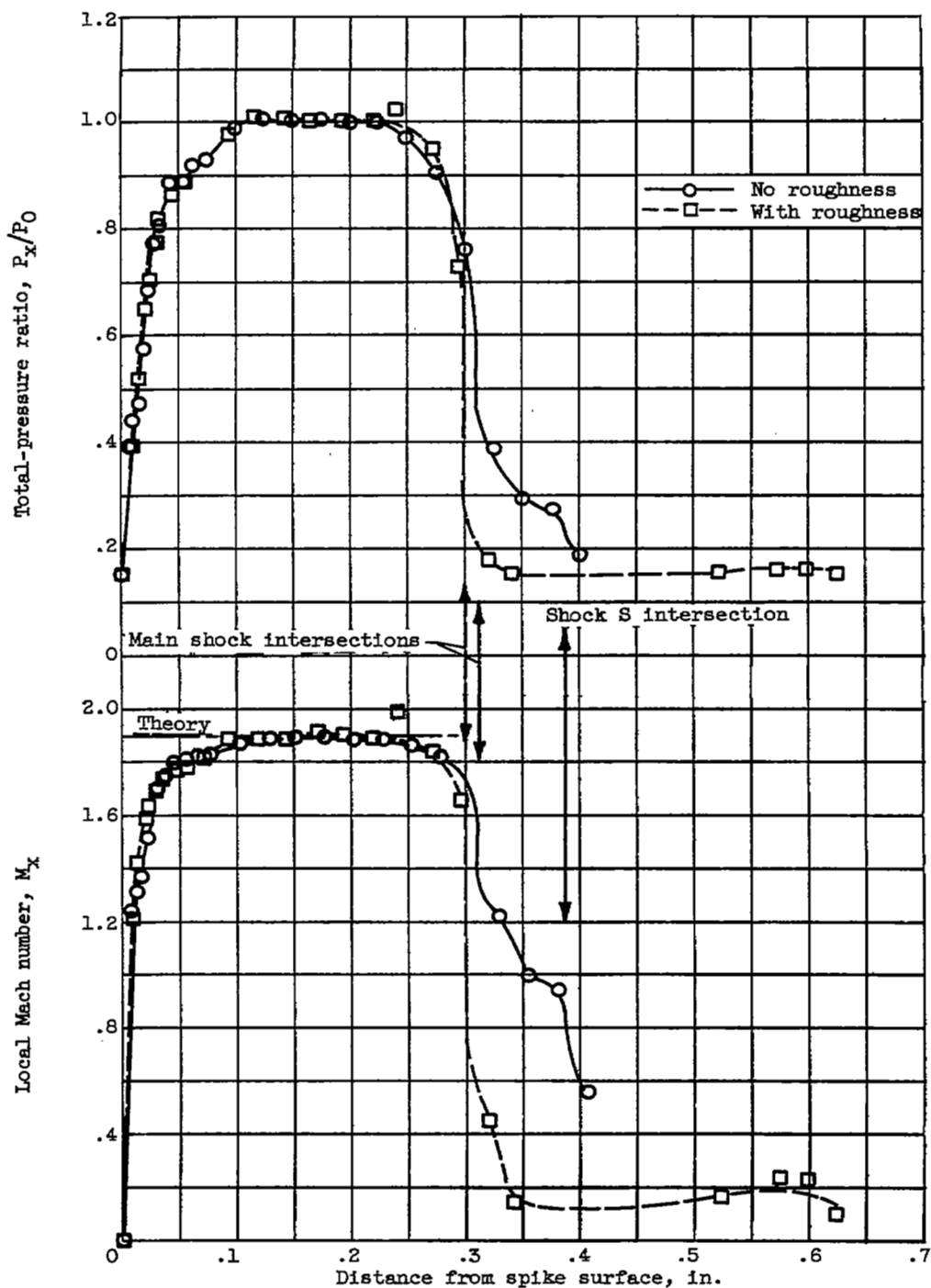
3320

CM-6 back

(a) Configurations A and A(R).

Figure 11. - Total-pressure and Mach number profiles for isentropic survey-spike configurations.

(b) Configurations B' and B'(R).

Figure 11. - Continued. Total-pressure and Mach number profiles for isentropic survey-spike configurations.
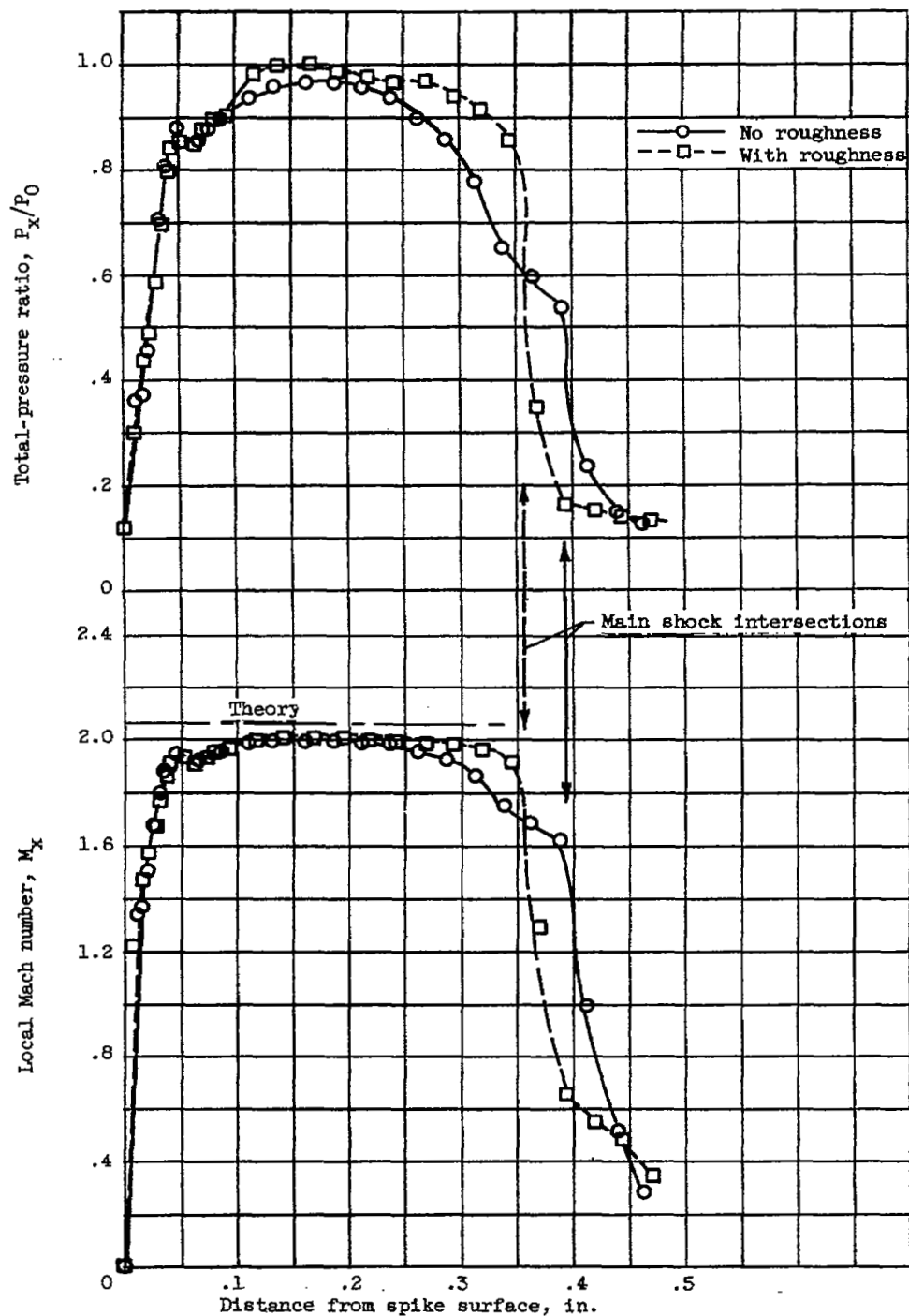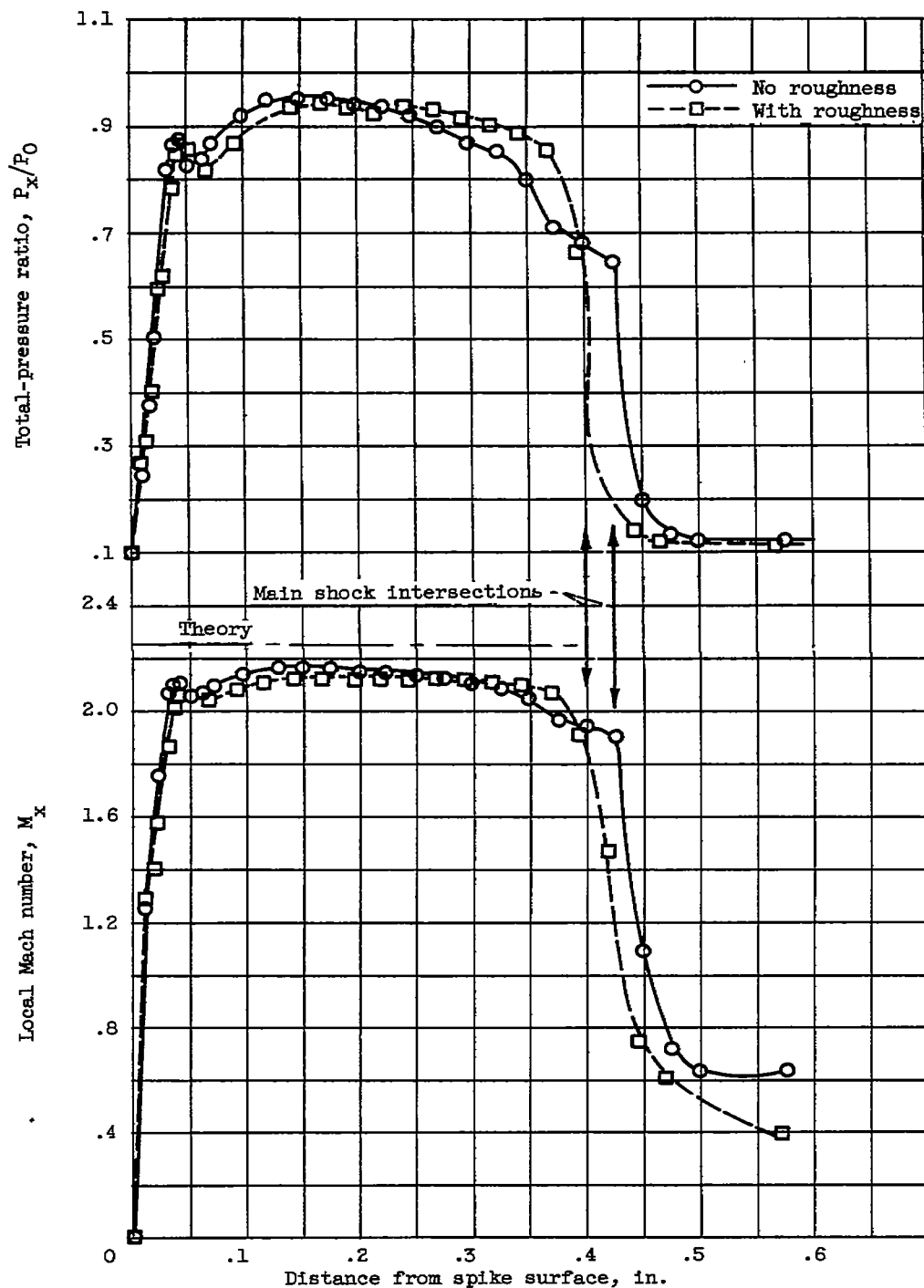
3320

(c) Configurations C' and C'(R).

Figure 11. - Continued. Total-pressure and Mach number profiles
for isentropic survey-spike configurations.

(d) Configurations D' and D'(R).

Figure 11. - Continued. Total-pressure and Mach number profiles
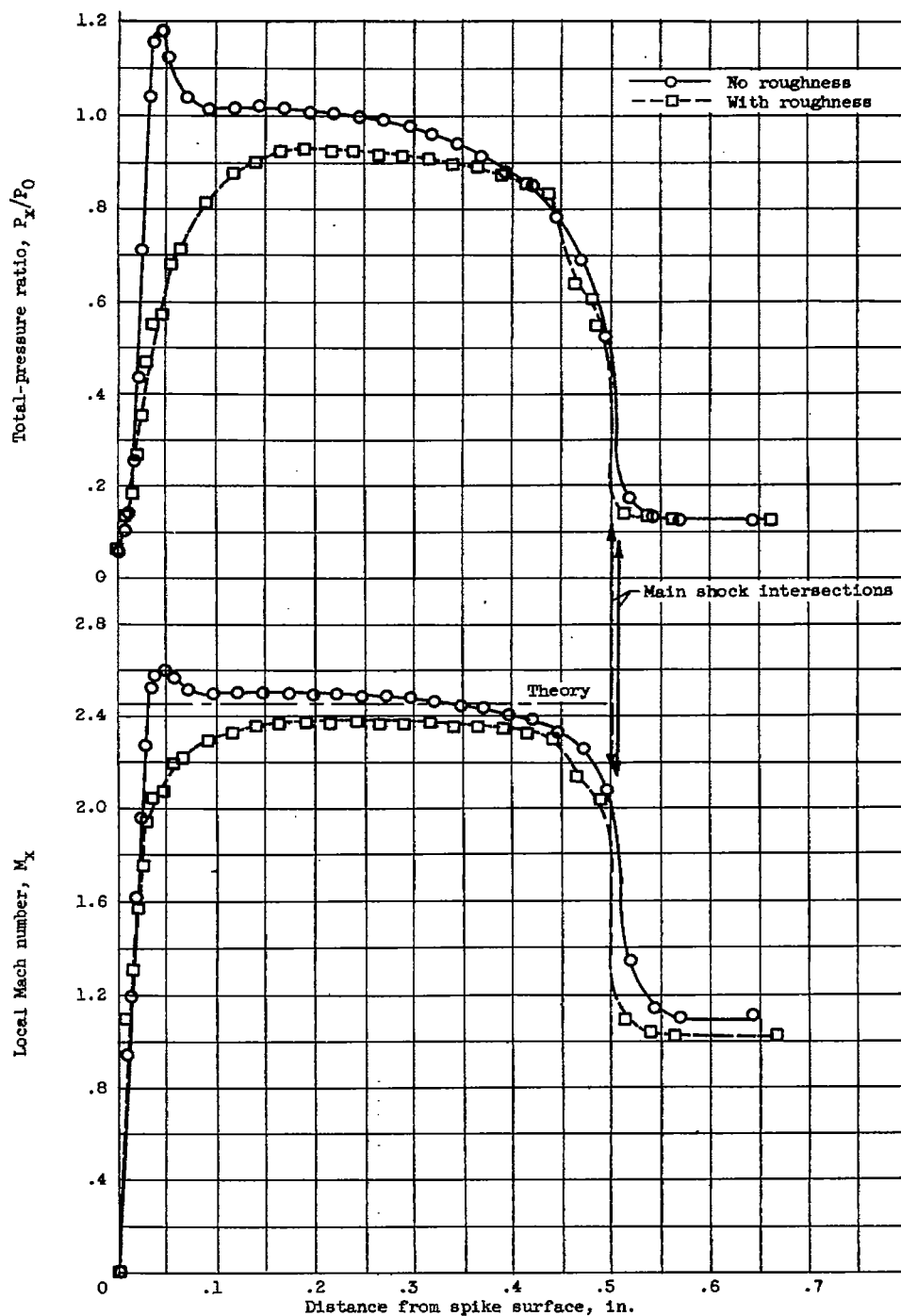for isentropic survey-spike configurations.

3320

(e) Configuration E' and E'(R).

Figure 11. - Continued. Total-pressure and Mach number profiles
for isentropic survey-spike configurations.

(f) Configurations F' and F'(R).

Figure 11. - Concluded. Total-pressure and Mach number profiles for isentropic survey-spike configurations.

Vortex lines

Strong shock

Shock S intersection

$M_0 = 3.85$

Choking

1

1

5

2

Normal shock

Shock reflection

5-6° Compressive turning

6

4

$M_2 = 3.0$

$\lambda = 12.6°$

Shock S

Main shock intersection

Survey plane

7

$M_7 = 1.7$

49.5°

Spike surface

Compression waves off spike

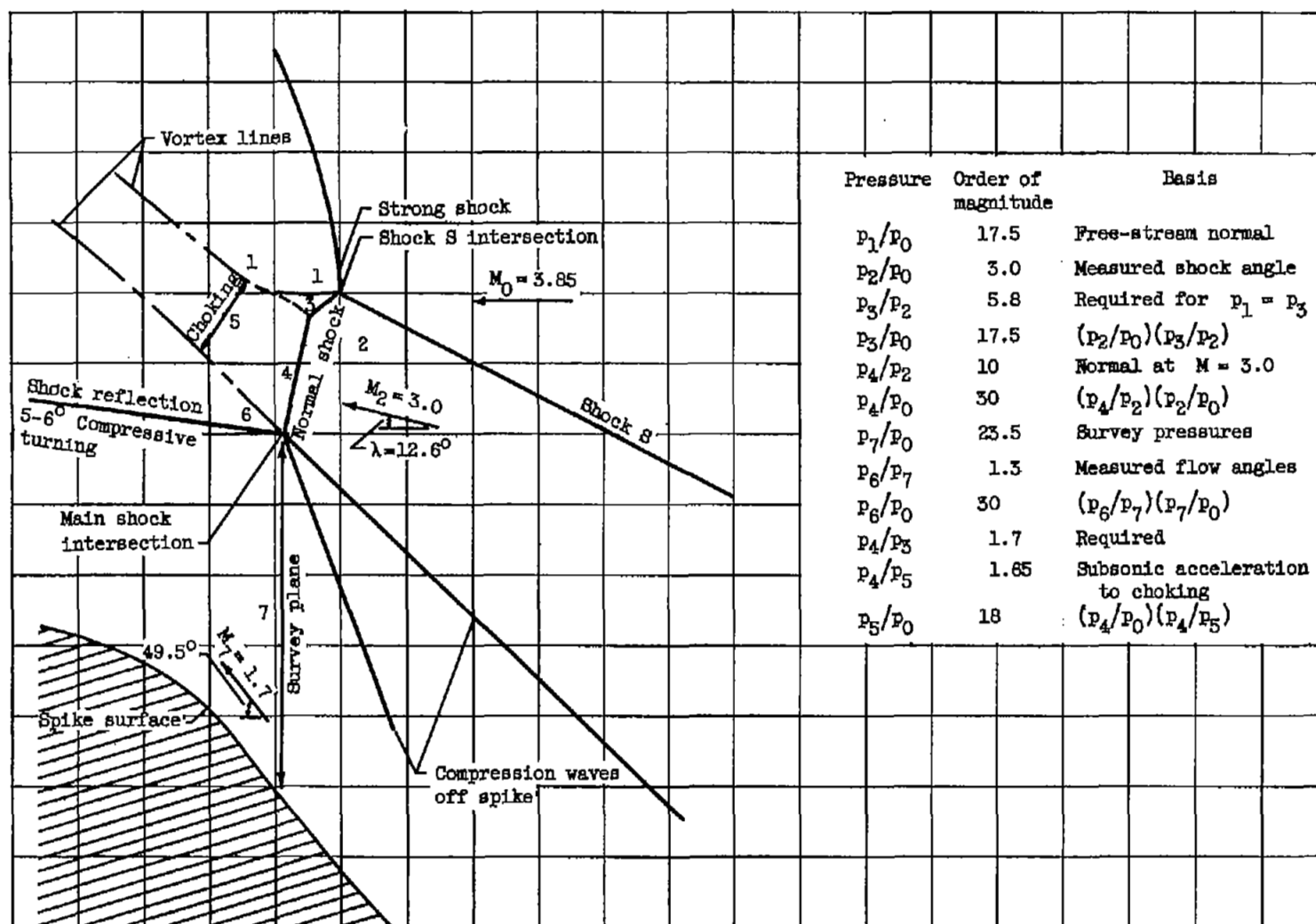| Pressure	Order of magnitude	Basis
p_1/p_0	17.5	Free-stream normal
p_2/p_0	3.0	Measured shock angle
p_3/p_2	5.8	Required for $p_1 = p_3$
p_3/p_0	17.5	$(p_2/p_0)(p_3/p_2)$
p_4/p_2	10	Normal at $M = 3.0$
p_4/p_0	30	$(p_4/p_2)(p_2/p_0)$
p_7/p_0	23.5	Survey pressures
p_6/p_7	1.3	Measured flow angles
p_6/p_0	30	$(p_6/p_7)(p_7/p_0)$
p_4/p_3	1.7	Required
p_4/p_5	1.65	Subsonic acceleration to choking
p_5/p_0	18	$(p_4/p_0)(p_4/p_5)$

Figure 12. - Experimental and analytical approximation of shock structure and flow fields obtained for configuration A of isentropic survey spike.
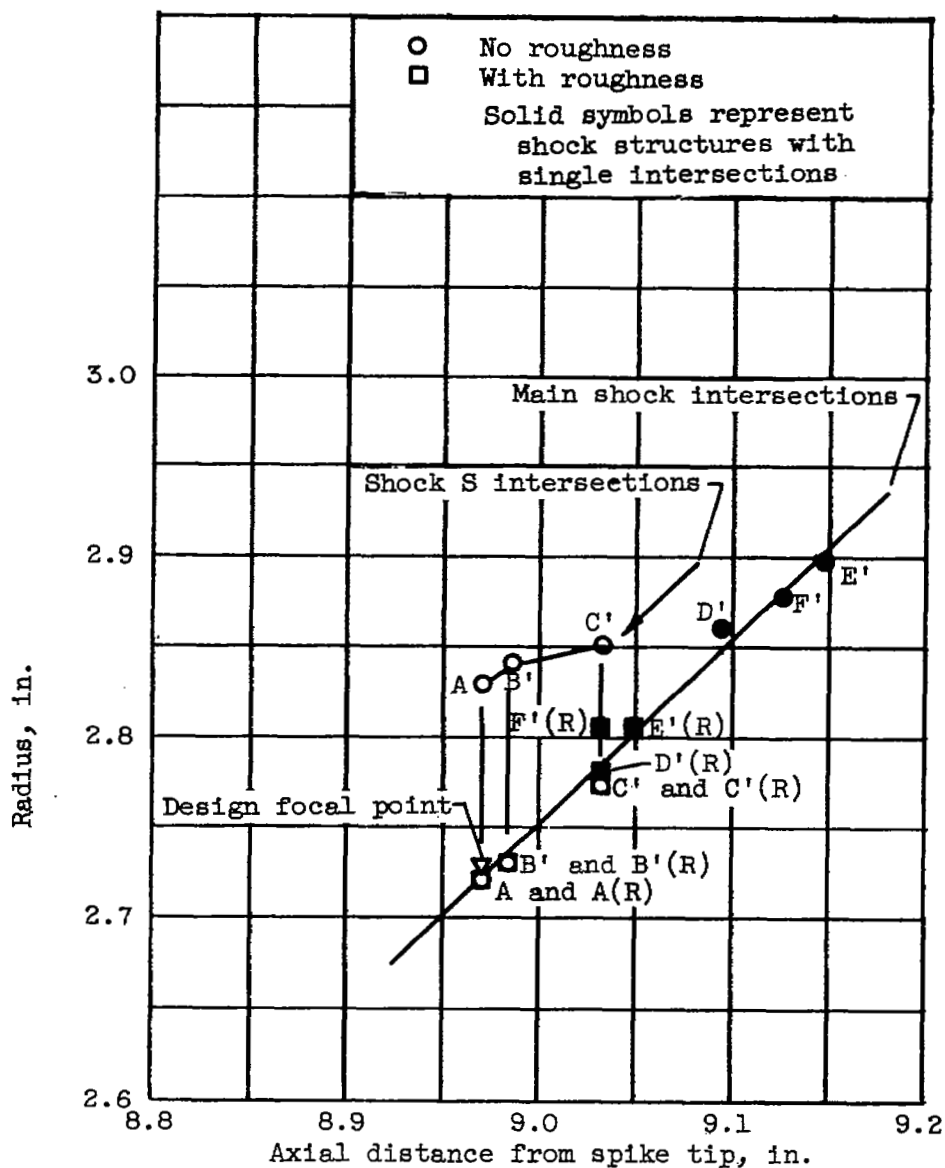
Figure 13. - Relative positions of shock inter-
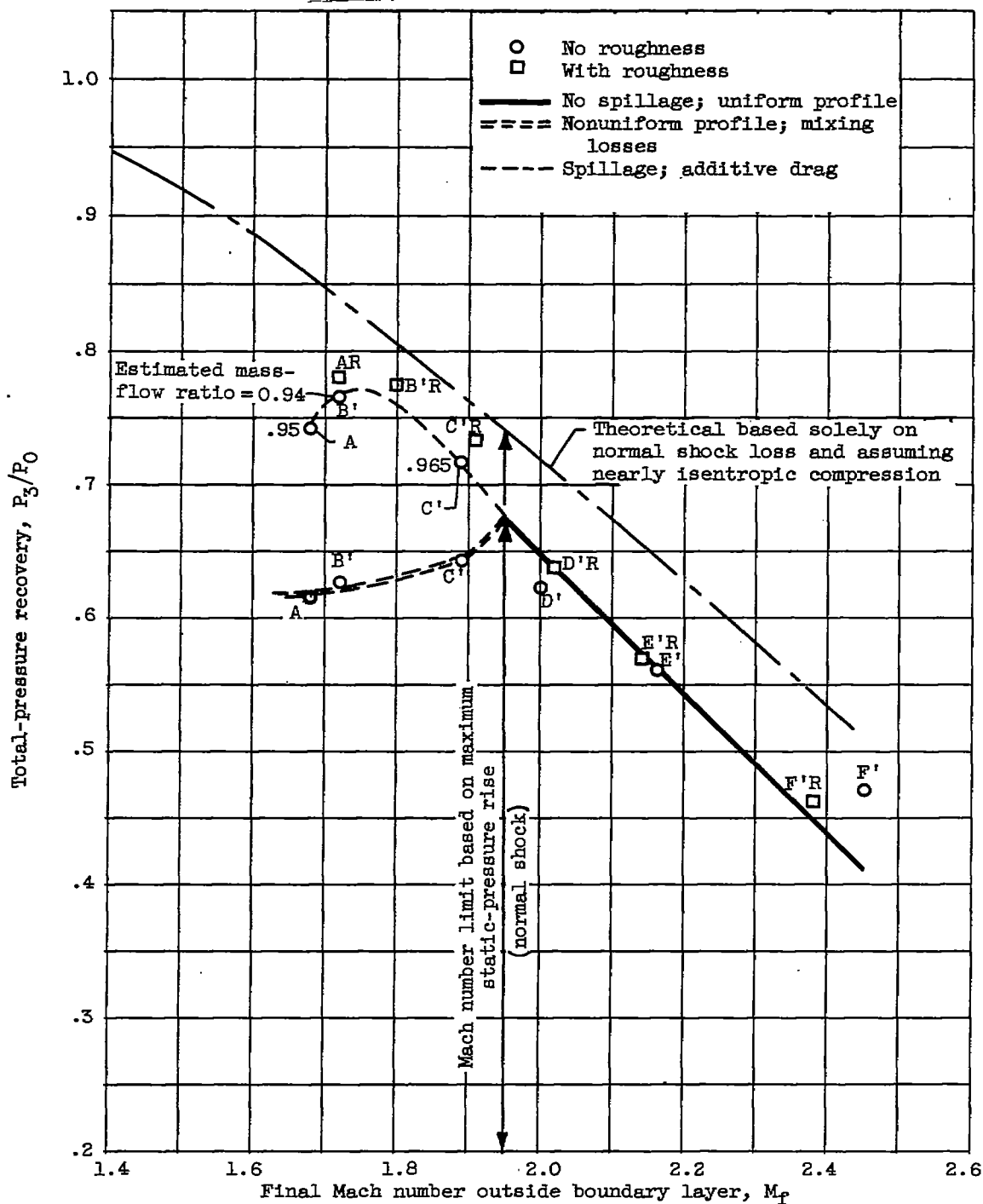sections encountered in survey plane.

Figure 14. - Summary of potential pressure recoveries available for all-
external-compression inlets designed to accommodate flow fields of vari-
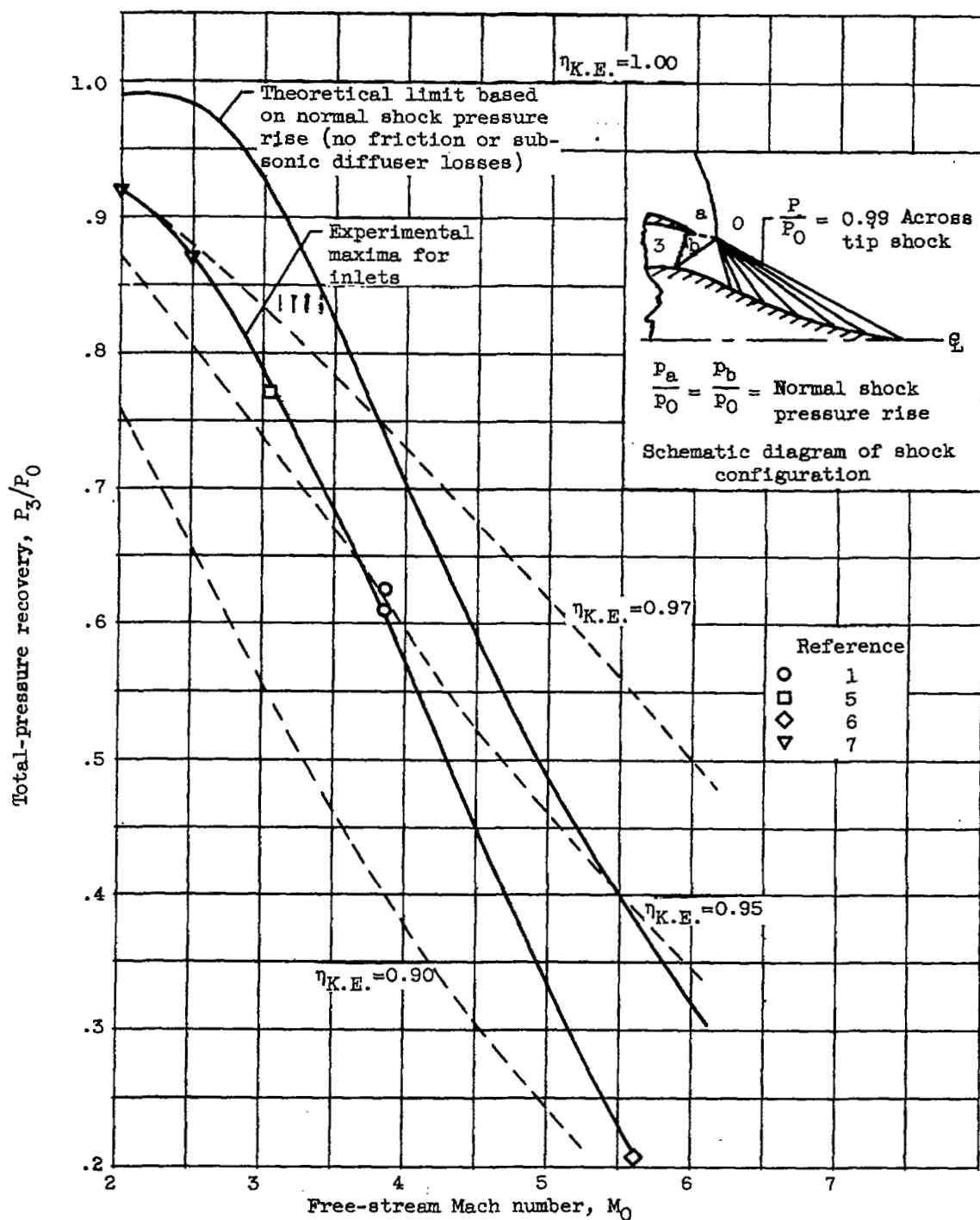ous isentropic spikes.

Figure 15. - Comparison of current experimental maximum recoveries
with theoretical limits for all-external-compression isentropic
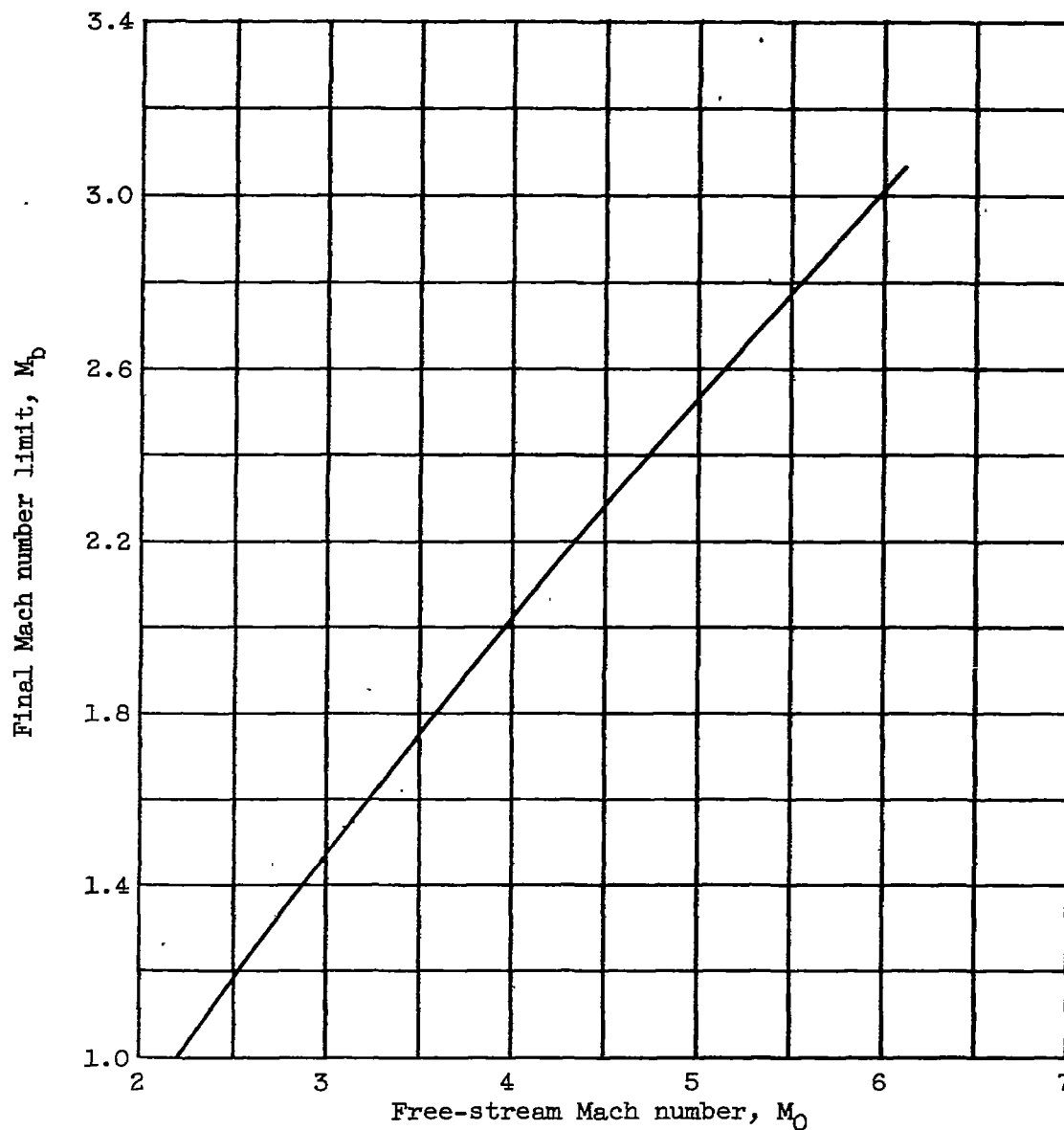inlets at several Mach numbers.

3320

Figure 16. - Effect of free-stream Mach number on final Mach number limit.